Journal of Hazardous Materials, 24 (1990) 1–38
Elsevier Science Publishers B.V., Amsterdam — Printed in The Netherlands

DENSE GAS REMOVAL FROM A VALLEY BY CROSSWINDS

GARY A. BRIGGS*, ROGER S. THOMPSON and WILLIAM H. SNYDER**

Atmospheric Sciences Modeling Division, Atmospheric Research and Exposure Assessment Laboratory, U.S. Environmental Protection Agency, Research Triangle Park, NC 27711 (U.S.A.)

(Received April 4, 1989; accepted in revised form February 5, 1990)

Summary

Wind tunnel experiments were made to determine how rapidly dense gas trapped in a topographic depression could be removed by an entraining crosswind. The two-dimensional outflow volume flux, v_o, was assumed equal to the inflow rate during 92 steady-state experiments with CO_2 continuously supplied into the bottom of two-dimensional, V-shaped valleys. As predicted by theory, at large Reynolds numbers it was found that $v_o \propto U_s^3/g_i'$, where U_s is the speed just above the dense gas pool and g_i' is gravity times the relative density difference. The width of the pool, w, does not affect v_o when the primary Froude number $\leqslant 1$, except at low Reynolds numbers; in this case the data suggest $v_o \propto (U_s w \kappa)^{1/2}$ as an asymptote, where κ is the molecular diffusivity. A universal relationship is suggested for v_o bridging these two asymptotes

Transient experiments were conducted by filling a valley with dense gas, turning it off, then quickly removing a sliding cover; v_o was measured as a function of time with an array of samplers downwind. These experiments essentially confirmed predictions based on the steady-state results, even when SF_6 was substituted for CO_2. Insertion of a flat floor into the valley had only minor effects on $v_o(t)$ until the pool level subsided almost to the floor level. Substantial changes in the removal process were observed for the few tests run at Froude numbers exceeding unity.

1. Purpose and scope

Clouds containing toxic vapors or mist from accidental releases, such as tank ruptures, are often denser than air, either because of high molecular weight gases or because of cooling due to flashing, evaporation, or expansion of gas from high pressure storage. When a heavier-than-air gaseous release occurs in or near a topographic depression there exists the possibility of pooling of the gas, that is, temporary trapping of the gas cloud in the depression. During pooling the dilution of the cloud by air through diffusion is greatly reduced or even arrested. When the released cloud is toxic and the low lying area contains

*On assignment from the National Oceanic and Atmospheric Administration, U.S. Department of Commerce.

** To whom correspondence about this paper should be addressed.

homes or workplaces, the potential for harm is greatly increased by the trapping. Because railroads, storage yards, processing plants, and homes are often situated in valleys, the hazardous situation described above could occur in any industrialized region that is not virtually flat.

A large, dense, toxic cloud released in a narrow valley could lead to particularly long exposure to high concentrations of the toxic material. The dose received is also highly dependent on meteorological conditions, especially on the wind speed and direction. In nearly calm, night-time conditions, the time to remove the dense cloud from the valley can be many hours, as will be shown; in extreme cases, the cloud will linger or drift with the drainage flow until an increase in wind speed or sunrise occurs. During daytime heating, the removal of the cloud is hastened by its loss of negative buoyancy as heat is absorbed from the surface (this situation is considered briefly in Section 9).

The purpose of this paper is to quantify the assessment of the removal rate of a dense gas from a valley due to "flushing", that is, entrainment into a crossflow of ambient wind. To this purpose, we carried out a series of laboratory experiments using carbon dioxide, CO_2, and sulfur hexafluoride, SF_6 (specific densities $\simeq 1.5$ and 5, respectively) introduced into two-dimensional, V-shaped valleys set into the floor of a neutrally stratified, boundary-layer wind tunnel. The valley axis was horizontal and perpendicular to the flow direction. The results show that the removal rate is strongly dependent on wind speed.

Research concerning the general problem of mixing between a lighter fluid moving over a heavier fluid has been surveyed by Christodoulou [1]. Experimental work was begun at the U.S. National Bureau of Standards by Keulegan [2] in 1949 using fresh water flowing over a sugar solution; more extensive experiments were carried out in the same laboratory by Lofquist [3] in an apparatus using salt water flowing under a confined layer of fresh water. Another related class of flows is density currents, which were studied by Ellison and Turner [4] and others. We recently learned of two laboratory experiments which relate more directly to our problem of heavy fluid trapped in a depression. König [5] released SF_6 in a wind tunnel upwind of various obstacles, including a rectangular channel perpendicular to the flow; only near-surface concentrations are reported. Seeto [6] measured the removal of salt solution from shallow, rectangular depressions spanning most of the width of a 0.6-m wide water channel; we examine his results in Appendix A.

Section 2 covers basic theoretical considerations pertaining to the expected entrainment rate and its possible dependence on wind speed, cloud density, valley width (fetch) and Reynolds number (Re). The latter is important because of the low tunnel speeds required by our experiment. Section 3 describes the tunnel–valley configurations, instrumentation, and procedures followed during the course of our two types of experiments. The subsequent three sections give results of "steady-state" experiments, in which CO_2 gas was put in at a constant rate into the bottom of the valley through a porous bed. Mea-

surements were made at various wind speeds after a pool of dense gas formed and its concentration profile stabilized (implying that the flushing rate equaled the inflow rate); 92 tests were conducted at various combinations of Froude number (Fr) and dimensionless inflow (outflow) rate. Section 7 gives results of the "flushing" experiments, in which a covered valley was filled with dense gas; after the gas was turned off, a sliding cover was quickly removed from over the valley; the flux of dense gas just downwind of the valley was measured as a function of time until the valley was emptied. Section 8 is a summary, and in Section 9 our generalized results are applied to some hypothetical spill scenarios. Estimates are also made to show how flushing time is affected by gravitational spread of the gas along the axis of a level valley and by heating.

2. Theoretical considerations

In the situation to be addressed, dense gas pooled in a topographic depression is gradually removed by turbulent entrainment induced by a crosswind above the pool. Deep in the pool the dense gas remains unmixed with the ambient flow, until flushing reduces the pool depth, z_p, to a level near the bottom of the depression (hereafter referred to as "valley"). The concentration of the unmixed gas is C_i (its initial or inflow value) and its density is ρ_i. Its buoyancy relative to the ambient fluid, of density ρ_a, is g'_i, where we define $g'_i = g(\rho_i - \rho_a)/\rho_a$. We define z_p to be the height above the bottom of the pool where the local concentration $C = C_i/2$. Figure 1 is a cross sectional view of the above process, with the symbols for the main geometrically-defined variables.

The surface of the dense gas pool is scoured by an ambient wind of speed U_s, which is, in practice, difficult to define. There is a continuous gradient of gas speed from the highest unmixed level of the pool, where it is nearly zero, to

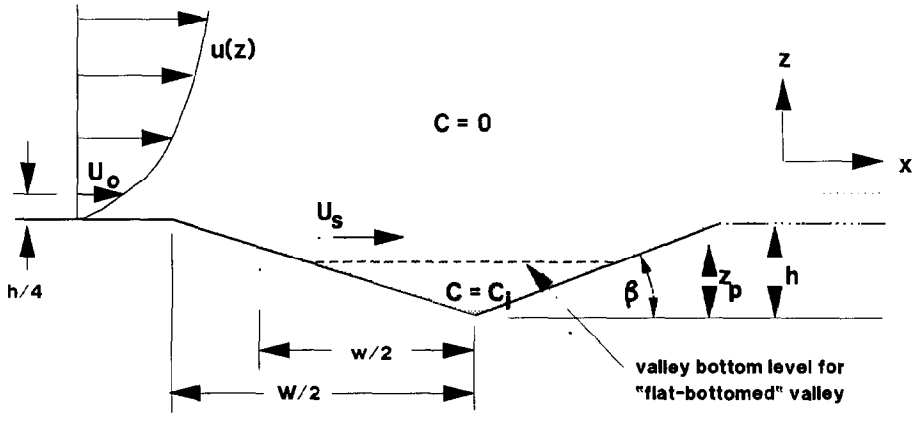

Fig. 1. Valley cross section, definition sketch.

well above the top of the pool. Furthermore, once the ambient flow passes from a uniform, flat, upwind fetch and begins to traverse the valley, the wind speed varies in the downstream (x) direction as well. If z_p is well below the top of a steep-walled valley, flow reversal may occur. ("Steep" in this case means that the slope, β, exceeds about 15°). To avoid the ambiguity associated with U_s, most parameters are defined using a reference wind speed, U_o, determined from a profile measured upwind of the valley influence. For simplicity, U_o is defined as mean wind speed at a height $h/4$ above the tunnel floor, where h is the total depth of the V-shaped valley. We assume that, at sufficiently high Reynolds number to avoid large effects of viscosity, speeds everywhere scale with U_o in similar flow situations (similar as regards z_p/h, Froude number, and valley shape).

To reduce flow complexity as much as possible, a two-dimensional valley was modeled with uniform cross section in the lateral (y) direction. Valley "length", in this discussion, refers to the y-direction, while "width" refers to valley size in the x-(along wind) direction. To accommodate as large a valley as possible in the wind tunnel, the valley length (cross-tunnel) was restricted to 1.4 times the valley width. This was considered sufficient to make any three-dimensional end effects small when measurements were taken near the center of the valley. A simple V-shaped valley cross section was chosen for the bulk of the experiments, with $\beta \simeq 21°$. However, we believe that our main results for flushing rate can be generalized to other terrain shapes if an appropriate U_s estimate can be made. Five sets of flushing experiments (five runs each) were carried out using a "flat-bottomed" valley, with just over half of the total valley width, W, fitted with a flat insert, a shape typical of older river valleys. As will be shown in Section 7, these experiments essentially confirmed the idea that the flushing rate, and by inference, the flow above the pool, is insensitive to the shape and depth of the pool below z_p.

Our primary interest was to measure and develop a prediction tool for the flushing rate per unit length (perpendicular to the wind), which can be defined as

$$v_o \equiv \int_0^\infty (C/C_i) u dz \tag{1}$$

measured at some distance immediately downwind of the valley. For the steady-state experiments, we merely assumed that outflow = inflow, with $v_o = v_i$, where v_i was the volume of inflow of dense gas per unit length of valley.

The primary factor affecting v_o is expected to be the ambient wind speed near the pool's surface, U_s. The airstream approaching the valleys was fully turbulent, adequately simulating a neutral boundary layer traversing a rough surface. However, this background turbulence was not strong enough to ac-

count for the observed entrainment: the estimated thickness of the entrainment layer, about 6 v_o/U_s, was 10 to 300 times larger than σ_w^2/g_i', the depth into the dense gas that turbulence with a vertical kinetic energy $\sigma_w^2/2$ could penetrate ($\sigma_w \simeq U_o/16$ in our boundary layer). Therefore, most of the entrainment must have been due to turbulence caused by the shear between the ambient and the relatively quiescent, dense gas.

Were no buoyancy involved, we might expect an entrainment velocity due to shear-generated turbulence, u_e, proportional to U_s, and a total flushing rate equal to this times the fetch over the interface, x: $v_o \propto u_e x \propto U_s x$. However, the amount of dense gas that can be picked up by the shear-generated turbulence is limited because the weight of the dense gas tends to stabilize the interface, eventually choking off any turbulence. We can make this process semiquantitative by considering the local entrainment layer Froude number, defined by $Fr_e = U_s^2/(g_i'\delta)$, where δ is the entrainment layer thickness. Initially, $v_o \propto U_s x$; as the mean transport speed in the entrained layer is proportional to U_s, we also expect $v_o \propto U_s \delta$. Then $\delta \propto x$. Therefore, at small x, Fr_e is very large, meaning that inertial forces overwhelm the buoyancy forces at this stage. However, when δ grows to the point that $Fr_e \sim 1$, the stable density gradient is deep enough to prevent U_s-induced turbulence from penetrating further into the unmixed dense gas lying below the entrainment layer. This stabilizing distance, x_s, as well as the asymptotic δ, is proportional to U_s^2/g_i'. This gives $v_o \propto U_s^3/g_i'$.

The above scenario, with v_o becoming limited due to the heaviness of the entrained fluid, is consistent with the observations of a laboratory "surface jet" of Ellison and Turner [4]. The thickness of the mixed fluid grew almost linearly with distance at first, then slowed until the depth changed little with distance. As this happened, the turbulence in the mixed layer dampened out. Somewhat crude measurements of velocity profiles were made using cinematography and small plastic particles. Taking δ as the depth of the jet and U_s as the velocity of the top of the jet, minus half of the backflow velocity, they estimated that u_e became zero when $\delta g_i'/U_s^2 = Fr_e^{-1} \simeq 0.74$. However, Britter and Simpson's [7] results from observations of the head of gravity currents are consistent with their estimate of an asymptotic $Fr_e^{-1} \simeq 0.35$, based on Thorpe's [8] experiment, to be described below.

We note that our view and those of the above authors is fundamentally different from a common approach found in the literature as seen, for example, in the review of Christodoulou [1]. This approach does not recognize the dependence of u_e on fetch; instead, it assumes an averaged u_e proportional to U_s times a function of a bulk Richardson number, $g_i' L/U_s^2$, where L is a characteristic length defined variously by different authors (e.g., total flow depth, estimated boundary layer depth, etc.). This approach is compatible with ours only if $L \propto x$, which is, unfortunately, an uncommon approach.

Details of the process we are assuming are well illuminated by the experiments conducted by Thorpe [8]. Thorpe's photographs and measurements

were made in a very different fluid configuration, but one which nonetheless involved a horizontal density interface and a velocity shear. A 16-cm wide rectangular tube, 5 m long, was filled half with brine and half with water. The tube was held horizontal until all motion subsided, then quickly tilted about 8°, causing an up-tube gravitational acceleration in the (less dense) water and an equal down-tube acceleration in the brine. After a short, predetermined time, the tube was brought quickly back to horizontal, and measurements were begun. We interpret Thorpe's results for our flow by assuming that the situation at the midpoint of the entrainment layer, where $u = U_s/2$, is similar to that at the midpoint of the density gradient in Thorpe's experiments. We replace the time after flow initialization in his experiments with the time for traversal from the upwind edge of the dense gas pool, $x/(U_s/2)$. We also set U_s equal to the difference between the "free fluid" water and brine velocities outside the interacting layer.

In the first moments after flow initialization, waves began developing on the density gradient interface. When this interface thickness (a function of molecular diffusion and the time after filling the tube) was initially quite small, so that $Fr_e \gg 1$, the wave amplitude grew at a rate approximated by $0.06\ U_s$. The waves reached a limiting amplitude $\simeq (1/4) U_s^2/g_i'$ and began to break; photographs show turbulence developing at this time. (Flow visualization runs in our experiment, using smoke released near the top of the pool, confirmed the existence of choppy, breaking waves at tunnel speeds greater than about 0.3 m/s.) Then the thickness of the fine structure (turbulence) grew at about the same rate as the initial wave amplitudes, finally filling a layer of constant thickness $\delta \sim 0.4\ U_s^2/g_i'$. Thereafter, the turbulence became more and more fine structured, consistent with the idea that the larger eddies are extinguished more rapidly by a stable density gradient. The final profiles approximate a linear decrease in density and a linear increase in velocity through a layer of thickness $\delta \sim 0.3\ U_s^2/g_i'$, although there are slight "tails" extending this gradient. As a first approximation for our flushing rate, we would therefore guess $v_o \simeq \int_0^\delta (z/\delta) U_s (1 - z/\delta) dz$, where z (in this usage only) is the height above the bottom of the linear layer, $(z/\delta) U_s$ is the local transport speed, and $(1 - z/\delta)$ is the local relative concentration. This gives $v_o \simeq U_s \delta/6 \simeq 0.05\ U_s^3/g_i'$ for the near-linear layer.

This whole process required a time of about $10\ U_s/g_i'$, which translates to a traverse $x_s \simeq 5\ U_s^2/g_i'$, in our case. (Note that this distance is about $15\ \delta$.) For a dense gas pool completely filling a valley, we can take $U_s \simeq U_o$ and say that this entrainment-limiting situation will occur before the flow traverses the pool if $5U_o^2/g_i' < W$, or $Fr_w = U_o^2/(g_i' W) < 0.2$. The primary Froude number tabulated for our experiments if $Fr_o \equiv U_o^2/(g_i' h)$, which approximates $5\ Fr_w$ for our valleys. Thus, we expect entrainment limiting at full pool level in our ex-

periments if $Fr_o < 1$, a condition which we observed except in some of the flushing experiments (Section 7). If $Fr_w > 0.2$, we would expect $v_o = (U_o^3/g_i')$ times a function of Fr_w, becoming proportional to $U_o W$ at very large Fr_w. Note also that the relative thickness of the limited entrainment layer, δ/h, is about 0.3 Fr_o for the full pool case. For $Fr_o \gg 1$, we expect immediate sweepout of the entire depth of the pool, consistent with Bell and Thompson's [9] result for (continuously) density-stratified valleys.

When the dense gas pool does not fill the valley, the pool is less wide; in the case of the V-shaped valley, the pool width $w = WZ_p$, where $Z_p = z_p/h$. However, $U_s < U_o$ at $Z_p < 1$ owing to the sheltering effect of the valley. It follows from the U_s/U_o versus Z_p relationship for our valleys, estimated in Section 6, that 5 $U_s^2/g_i' < w$ at all measured levels of Z_p if $Fr_o < 1$. That is, the pool width is sufficient for entrainment limiting regardless of pool depth if $Fr_o < 1$.

For our steady-state experiments the outflow was balanced by a constant inflow rate, $v_o = v_i$. In this case, we expected that pool parameters such as Z_p would be functions of a nondimensional variable involving v_i, as well as Fr_o. This expectation was substantiated. In carrying out these experiments, we targeted standard values of $V_o = v_i/(U_o h)$, comparing v_i to a (full concentration) outflow of thickness h. (Note from Table 3 that V_o was quite small, 0.002 to 0.03.) However, for data analysis we found $V' \equiv v_i/(U_o^3/g_i') = V_o/Fr_o$ more useful because of its more direct relationship with the prediction $v_o \propto U_s^3/g_i'$. (We will freely substitute v_o for v_i in all results from the steady-state experiments.)

Because of our modeling scale and the need to reduce U_o to obtain a realistic range of Fr_o (0.1 to 1 was our targeted range), Reynolds number (Re) effects were an additional possibility. If this number is too small, molecular viscosity and diffusivity can significantly influence both the wind field and the turbulent entrainment. To better develop Re criteria, we ran nearly identical experiments, in terms of Fr_o and V_o, in three different valley sizes, with $h = 9$, 14, and 25.4 cm. At a fixed value of Fr_o, all Re are proportional to $h^{3/2}$. The effectiveness of various Reynolds numbers as an additional parameter is discussed in Section 5 and in the appendix.

3. Experimental details

The experiments were conducted in the Meteorological Wind Tunnel of the EPA Fluid Modeling Facility in Research Triangle Park, NC. This open circuit, low speed wind tunnel was designed for simulating neutral atmospheric boundary-layer flows. The test section is 18 m long, 3.7 cm wide, and 2.1 m high. A thorough description of the Meteorological Wind Tunnel can be found in Snyder [10].

Velocity measurements were made with a TSI, Inc. hot-film anemometer. Measurements were made by using both an X-array hot-film probe and a single film probe. Calibration of the anemometer at the low wind speeds used for this

study was difficult. At the lowest speed settings, calibration velocities were determined by timing the travel of smoke puffs over a predetermined distance in the wind-tunnel test section. At a wind-tunnel tachometer setting of 40 ($U_o \simeq 0.2$ m/s) the error in U_o could be as much as 10% and for settings of 60 ($U_o \simeq 0.4$ m/s) and greater, about 5%. (The tachometer indicates the fan speed.) The response of the hot-film anemometer in CO_2 was checked in a TSI calibrator by calibrating in air and then, using that calibration, obtaining indicated velocities in known speeds of pure CO_2. The indicated velocities agreed with the known values within the limit of errors in the calibration except at very low velocities. These results are in agreement with those of Pitts and McCaffrey [11], which show nearly identical calibration fits for a hot-film anemometer calibrated in air and in pure CO_2. It was assumed that for mixtures of CO_2 and air the response of a hot-film would not be much different than for either of the pure gases.

Concentrations of the dense gas were determined by adding a known fraction of a tracer gas (ethane, 99% pure) to the dense gas. Concentrations of the tracer were obtained with flame ionization detectors (Beckman, model 400 hydrocarbon analyzers). Ambient samples were drawn through a rake of sampling tubes (0.24 cm o.d.), each connected to an analyzer via Teflon tubing. The response time of this system was about one second. The hydrocarbon analyzers were used mostly to obtain mean concentrations, so the one-second time constant was acceptable. For time-dependent flux measurements downwind of the valley, this response time was small compared to the flushing time of the valley (on the order of 30 seconds) and, in effect, helped in smoothing the data. Up to nine analyzers were used in a given experiment. These instruments have a linear response and were calibrated with "zero" air and a span gas (0.9% ethane). A check of midrange concentrations showed the instruments to measure concentrations to within 5%.

Data from all instruments were collected with a personal computer through an analog-to-digital interface. Anemometer data were typically averaged for a sampling period of 2 min at a sampling rate of 500 samples per second. Steady-state concentration data were also collected for 2-minute sampling periods but at a rate of 20 samples per second. Transient concentration data were also obtained at a sampling rate of 20 samples per second.

The boundary layer used for all experiments was initiated by tripping the flow with a 15.3 cm high fence across the floor of the test section, 65 cm downwind of its entrance. The floor surface of the test section was covered with Sanspray (a commercial construction material consisting of plywood covered with small stones adhered with epoxy). The characteristic roughness element (stone) size was 1 cm equivalent diameter. This configuration produced velocity and turbulence intensity profiles for various wind speeds as shown in Fig. 2, which are typical of a neutral atmospheric boundary layer. To obtain the Froude numbers desired for these experiments, very low wind speeds were re-

quired. The vertical profiles of velocity and turbulence intensity were similar except at tachometer settings below 50, as can be seen in Fig. 2. Only one series of steady-state experiments was conducted at such a low speed. All others were at settings of 50 or greater. For these, the $z = 1$ to 10 cm segment of the velocity profiles approximate a log law with an effective roughness length of the order 0.005 cm. The vertical coordinate, z, was always measured from the top of the surface roughness.

Density differences were obtained by releasing a heavier-than-air gas (either CO_2 or SF_6) mixed with the hydrocarbon tracer (nominally 0.5% by volume). The flow rates of each gas were measured and monitored with Meriam laminar flow elements. A Brooks flow calibrator (rated accuracy 0.5%) was used to determine the set points for pressure drops across the laminar flow elements.

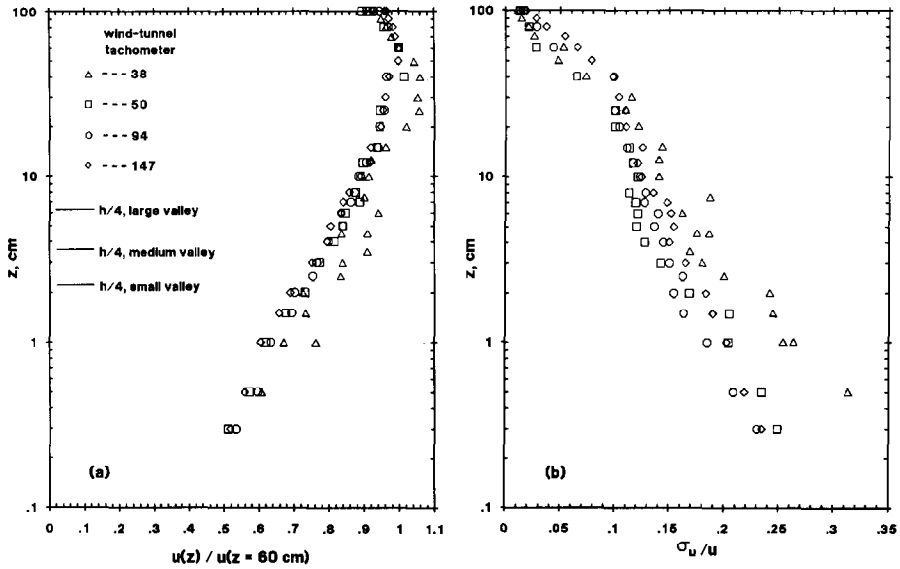

Fig. 2. Vertical profiles of (a) approach flow mean velocity and (b) longitudinal turbulence intensity. Heights defining U_o for each valley model are identified in (a).

TABLE 1

Valley model dimensions, cm

Valley	L	W	h
Small	71	50	9.0
Medium	99	70	14.0
Large	200	140	25.4
Sliding door	100	68	12.5

Checks of the flow rates before and after each series of experiments showed the flow rates to be steady and repeatable to within 1%.

Four valley models were used. All had triangular cross sections which were oriented perpendicular to the flow. Their surfaces were made to correspond to

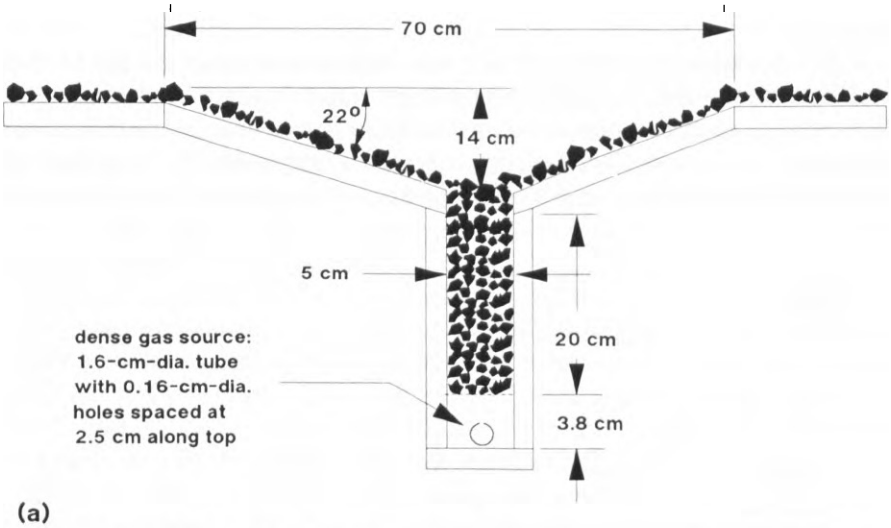

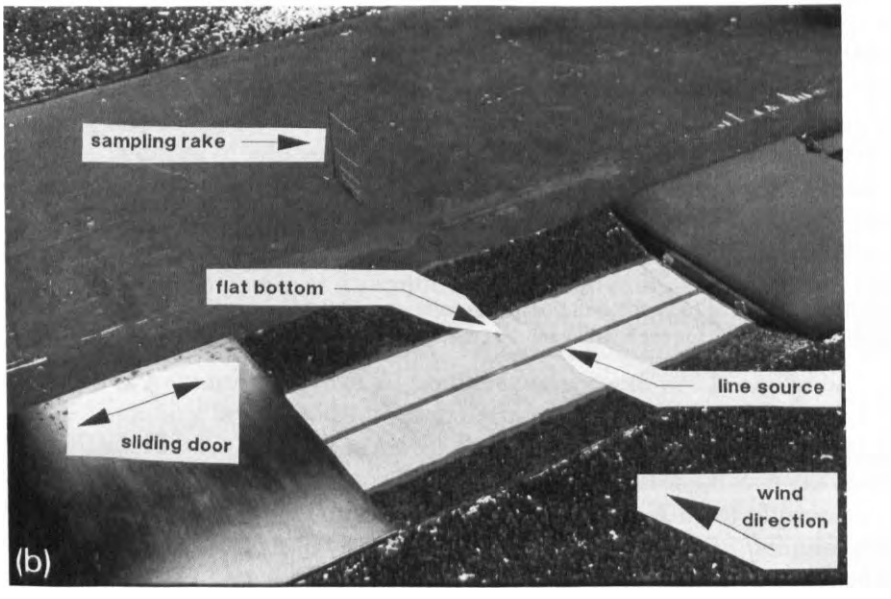

Fig. 3. Valley models: (a) cross section of medium valley model, (b) photo of sliding-door valley model with flat bottom insert in place; doors are open. Note the gas sampling rake downstream of the valley.

TABLE 2

Parameters used in flux calculations

j	z_j (cm)	Δz_j (cm)	$u(z_j)$ at each wind-tunnel tachometer setting, cm s^{-1}			
			160	128	102	82
1	0.1	0.21	40	30	25	19
2	0.3	0.21	59	47	36	29
3	0.6	0.42	71	56	43	35
4	1.2	0.84	68	53	53	41
5	2.4	1.68	90	77	59	47
6	4.8	3.36	107	87	67	49
7	9.6	6.72	120	96	75	58
8	19.2	13.44	134	108	84	-

the roughness of the wind tunnel floor by covering them with stones of the same size. The slope of the valley walls was about 21°. The dimensions of the valley models are listed in Table 1 and the cross-section of the middle valley is shown in Fig. 3(a). Each of these valleys had a line source to supply the dense gas along the valley bottom. To provide a nonjetting, uniform influx of dense gas, a rectangular box of stones (as used for covering the model surface) was attached to the bottom of each of the three valley models used in the steady-state experiments. A perforated pipe supplied the dense gas along the length of the bottom of these boxes. Steady-state experiments were performed by setting the flow rate of dense gas into the valley and measuring the vertical profile of tracer concentration above the valley center after the profile stabilized.

For transient flushing experiments, a fourth valley model was built with a pair of sliding doors to form a lid that met at the middle of the tunnel; see Fig. 3(b). The doors moved along the length of the valley and could be opened from outside the tunnel by pulling a rope connected to the doors through a pulley system. The line source for this valley was simply a perforated pipe placed along the bottom of the valley. These experiments were conducted by filling the valley with a dense gas and then quickly (in less than 1 second) opening the doors. The flushing experiments were repeated with a modified version of this 12.5 cm deep valley. A flat, false bottom (with the line source imbedded in a slot) was installed across the valley to produce a flat-bottomed valley with a depth of 5.5 cm.

The transient experiments were conducted to determine the flux of dense gas leaving the valley as a function of time after opening the sliding doors. To determine the flux, a vertical rake of eight sampling ports was located 36 cm downwind of the lee edge of the valley. The time histories of the concentration of tracer at each of the sampling heights were recorded from the time the slid-

ing doors were opened until the concentrations dropped to background levels. The time-dependent flux of dense gas from the valley was determined by computing the flux through a vertical plane downstream of the valley by numerical integration using a discrete form of eqn. (1):

$$v_o(t) = C_i^{-1} \sum_{j=1}^{N} C_j(t) u(z_j) \Delta z_j \tag{2}$$

where $v_o(t)$ is the outflow flux of dense gas per unit length of the valley, $C_j(t)$ is the concentration measured at height z_j, $u(z_j)$ is the mean wind speed at height z_j, Δz_j is the thickness assigned to layer j, C_i is the initial concentration of the dense gas in the valley, and N is the number of levels (7 or 8).

Experiments were run at four wind speeds (wind-tunnel tachometer settings of 82, 102, 128, and 160) using CO_2 and one speed (tach=160) using SF_6. Values of $u(z_j)$ for each wind speed and Δz_j are listed in Table 2. These wind speeds were measured at the position of the concentration sampling ports before their installation and in the absence of dense gas. Time histories of velocity at $z=0.5$ and 2.4 cm taken during flushing situations indicated only a slight decrease in wind speed as the CO_2 cloud passed. Thus, use of the wind speeds measured in the absence of the dense gas in eqn. (2) may cause a slight overestimation of the flushing rate (5 to 10% at count 82 and much less at the higher counts). For each experiment, five realizations were performed and averaged to obtain a representative $v_o(t)$.

4. Steady-state experiments

The purpose of our steady-state experiments was to study the entrainment process under controlled, known conditions, during which it could be assumed that the outflow flux was equal to the inflow rate, an easily measured quantity ($v_o = v_i$). Then we could explore how the dimensionless v_i or v_o relates to Froude number and how this relationship is affected by several different Reynolds numbers, in a search for a criterion for adequate simulation of full-scale events. This section presents a tabulation of the results. Section 5 presents analyses of the data for Reynolds number effects and Section 6 developes entrainment rate relationships.

A total of 92 steady-state runs with mid-pool concentration profile measurements was obtained; 46 of these were done in the "medium" valley (70 cm wide), while 23 runs each were done in the "large" and "small" valleys (140 cm and 50 cm wide). The procedure generally followed was to set v_i at a fixed value and to run a series at two to six different wind speeds. The tunnel tachometer was set at values intended to obtain standard values of $Fr_o \equiv U_o^2/(g_i' h)$ for all three valleys; thus, the targeted U_o values were proportional to $h^{1/2}$, producing Reynolds numbers that were proportional to $h^{3/2}$ at fixed values of Fr_o and dimensionless v_i. The v_i settings were also varied to target

standard values of $V_o \equiv v_i/(U_o h)$, approximately logarithmically spaced. We started with the largest valley, because it required the largest v_i, with the largest inflow rate we could easily obtain from three cylinders of CO_2. Tunnel wind speeds were then found that produced steady-state pool depths $z_p \simeq 0.3$, 0.6, and 0.9 h. The corresponding Fr_o and a set of decreasing V_o values were used to construct a table of target values.

The medium valley explorations were the most complete, filling in most possibilities between the limits of "overflow" ($C/C_i > 0.1$ at top of valley), shallow pool depth, minimum tunnel speed for adequate boundary layer simulation (~ 0.3 m/s), and $Fr_o < 1$. The large and small valley runs were chosen mostly to extend the Reynolds number dependence information, with Fr_o and V_o ranges that appeared to mark transition to fully turbulent (high Re) flow. Some small valley experiments at high Re were chosen to extend the range of V_o upward, the demand for v_i being only 0.21 times that for the large valley. Four Fr_o–V_o combinations were run twice. The resulting pool level variability ranged from 0.01 to 0.04 h and profile thickness (based on $C/C_i = 0.1$ to 0.9) variability ranged from 0.00 to 0.03 h.

Table 3 presents the most essential information for each steady-state run. The leftmost columns give the independent dimensional variables, h, v_i, and U_o, and the next three columns give three dimensionless variables. (For a given valley size and gas density, Re_o and Fr_o are not independent: $Re_o \equiv U_o h/\nu = Fr_o^{1/2} g_i'^{1/2} h^{3/2}/\nu$. However, Re_o varies strongly with valley size.) We used $g_i' = (44/28.9 - 1)980$ cm/s^2 = 512 cm/s^2 and $\nu = 0.15$ cm^2/s (the kinematic viscosity of air) in these calculations. We use several alternative dimensionless variables in the following sections, but they can be derived from these three. The rightmost columns are principal results. "C_{top}" gives the concentration measured at mid-valley at an elevation level with the top of the roughness of the tunnel floor. When it exceeds 10% or so, we assume an "overflow" condition, in which much of v_o results when dense gas is simply pushed out of the valley, rather than being picked up by turbulent entrainment, our main interest. This occurs mainly when $Z_p = z_p/h$ exceeds 0.9. Z_p is considered the most important dependent variable, because U_s/U_o and, therefore, the entrainment rate, varies markedly with pool depth. The C/C_i versus z/h profiles looked smooth and rather similar in most runs (see Fig. 7), except for variations in gradient thickness and steepness top-to-bottom. We chose to characterize these profile shapes with just the thickness (divided by h) from the $C/C_i = 0.1$ to 0.5 levels, ΔZ^+, and the 0.5 to 0.9 levels, ΔZ^-.

5. Determination of *Re* effects

Preliminary analyses of the tabulated results showed that, for all three valley sizes, for runs of nearly equal Z_p, there existed regions of larger Fr_o and V_o in which $V' = V_o/Fr_o = v_o g_i'/U_o^3 \simeq$ constant. This, together with the notion that

TABLE 3

Principal variables, steady-state CO_2 experiments

h (cm)	υ_i ($cm^2 s^{-1}$)	U_o ($cm\,s^{-1}$)	Fr_o	Re_o	V_o	C_{top} (%)	Z_p	ΔZ^+ (0.1–0.5)	ΔZ^- (0.5–0.9)
25.4	13.16	112.0	0.965	18965	0.00463	0	0.290	0.120	0.100
25.4	13.16	89.4	0.615	15138	0.00579	0	0.380	0.090	0.090
25.4	13.16	72.0	0.399	12192	0.00719	0	0.570	0.090	0.080
25.4	13.16	53.6	0.221	9076	0.00966	4	0.890	0.080	0.100
25.4	10.27	112.0	0.965	18965	0.00361	0	0.260	0.120	0.110
25.4	10.27	89.4	0.615	15138	0.00452	0	0.330	0.100	0.110
25.4	10.27	72.0	0.399	12192	0.00562	0	0.500	0.080	0.100
25.4	10.27	53.6	0.221	9076	0.00755	1	0.820	0.080	0.140
25.4	10.27	42.0	0.136	7112	0.00963	12	0.940	0.070	0.140
25.4	10.27	32.6	0.082	5520	0.01241	45	0.990	0.070	0.150
25.4	6.41	112.0	0.965	18965	0.00225	0	0.170	0.120	0.100
25.4	6.41	89.4	0.615	15138	0.00282	0	0.260	0.110	0.140
25.4	6.41	72.0	0.399	12192	0.00351	0	0.370	0.100	0.120
25.4	6.41	53.6	0.221	9076	0.00471	0	0.580	0.100	0.120
25.4	6.41	42.0	0.136	7112	0.00601	1	0.770	0.110	0.170
25.4	6.41	32.6	0.082	5520	0.00774	16	0.920	0.100	0.210
25.4	4.07	53.6	0.221	9076	0.00299	0	0.420	0.090	0.170
25.4	4.07	42.0	0.136	7112	0.00381	0	0.520	0.120	0.180
25.4	4.07	32.6	0.082	5520	0.00491	1	0.760	0.160	0.260
25.4	3.28	53.6	0.221	9076	0.00241	0	0.370	0.100	0.160
25.4	3.28	42.0	0.136	7112	0.00308	0	0.470	0.120	0.150
25.4	3.28	32.6	0.082	5520	0.00396	0	0.680	0.180	0.320
25.4	3.28	32.6	0.082	5520	0.00396	0	0.640	0.170	0.300
14	13.25	83.0	0.961	7747	0.01140	1	0.470	0.135	0.090
14	10.42	83.0	0.961	7747	0.00896	0	0.410	0.130	0.110
14	10.42	66.4	0.615	6197	0.01121	0	0.555	0.110	0.100
14	8.38	83.0	0.961	7747	0.00721	0	0.360	0.145	0.125
14	8.38	66.4	0.615	6197	0.00901	0	0.490	0.115	0.130
14	8.38	53.5	0.399	4993	0.01118	1	0.675	0.100	0.130
14	8.38	53.5	0.399	4993	0.01118	1	0.705	0.100	0.130
14	6.78	83.0	0.961	7747	0.00583	0	0.325	0.140	0.140
14	6.78	66.4	0.615	6197	0.00729	0	0.450	0.115	0.135
14	6.78	53.5	0.399	4993	0.00905	0	0.600	0.110	0.135
14	6.78	39.8	0.221	3715	0.01216	5	0.880	0.090	0.180
14	5.33	83.0	0.961	7747	0.00459	1	0.300	0.140	0.140
14	5.33	83.0	0.961	7747	0.00459	1	0.310	0.155	0.145
14	5.13	66.4	0.615	6197	0.00552	0	0.380	0.140	0.150
14	5.33	53.5	0.399	4993	0.00712	0	0.565	0.115	0.165
14	5.33	39.8	0.221	3715	0.00957	3	0.840	0.100	0.200
14	5.13	31.2	0.136	2912	0.01174	8	0.875	0.115	0.200
14	4.21	83.0	0.961	7747	0.00362	0	0.230	0.140	0.130
14	4.21	66.4	0.615	6197	0.00453	0	0.350	0.125	0.155
14	4.21	53.5	0.399	4993	0.00562	0	0.460	0.120	0.160
14	4.21	39.8	0.221	3715	0.00755	0	0.680	0.110	0.200
14	4.21	31.2	0.136	2912	0.00963	2	0.830	0.120	0.240
14	4.21	21.3	0.063	1988	0.01411	18	0.890	-	0.280

h (cm)	υ_i ($cm^2 s^{-1}$)	U_o ($cm\ s^{-1}$)	Fr_o	Re_o	V_o	C_{top} (%)	Z_p	ΔZ^+ (0.1–0.5)	ΔZ^- (0.5–0.9)
14	3.31	66.4	0.615	6197	0.00356	0	0.300	0.130	0.170
14	3.31	53.5	0.399	4993	0.00442	0	0.400	0.140	0.190
14	3.31	39.8	0.221	3715	0.00595	0	0.580	0.150	0.230
14	3.31	31.2	0.136	2912	0.00758	2	0.780	0.160	0.300
14	3.31	21.3	0.063	1988	0.01111	13	0.840	-	0.300
14	2.67	83.0	0.961	7747	0.00230	0	0.160	0.135	0.105
14	2.67	66.4	0.615	6197	0.00287	0	0.265	0.145	0.175
14	2.62	53.5	0.399	4993	0.00349	0	0.320	0.140	0.190
14	2.67	39.8	0.221	3715	0.00479	0	0.505	0.145	0.245
14	2.62	31.2	0.136	2912	0.00599	0	0.640	0.180	0.280
14	2.62	21.3	0.063	1988	0.00878	5	0.790	0.190	0.320
14	2.14	53.5	0.399	4993	0.00286	0	0.265	0.160	0.180
14	2.14	39.8	0.221	3715	0.00384	0	0.370	0.170	0.205
14	2.14	31.2	0.136	2912	0.00490	0	0.540	0.180	0.290
14	2.14	21.3	0.063	1988	0.00718	1	0.690	0.220	0.350
14	1.67	39.8	0.221	3715	0.00299	0	0.330	0.195	0.240
14	1.67	31.2	0.136	2912	0.00382	0	0.430	0.240	0.270
14	1.67	21.3	0.063	1988	0.00559	0	0.580	0.320	0.380
14	1.33	39.8	0.221	3715	0.00239	0	0.240	0.210	0.210
14	1.33	31.2	0.136	2912	0.00305	0	0.330	0.230	0.260
14	1.33	21.3	0.063	1988	0.00446	0	0.480	0.270	0.370
14	1.06	31.2	0.136	2912	0.00242	0	0.310	0.260	0.250
14	1.06	21.3	0.063	1988	0.00355	0	0.470	0.330	0.330
9	13.38	66.5	0.960	3990	0.02235	1	0.530	0.140	0.120
9	10.77	66.5	0.960	3990	0.01800	0	0.470	0.140	0.140
9	10.77	53.2	0.614	3192	0.02250	3	0.790	0.130	0.130
9	10.77	42.9	0.399	2574	0.02790	15	0.910	0.110	0.160
9	8.60	66.5	0.960	3990	0.01436	1	0.420	0.160	0.120
9	8.60	53.2	0.614	3192	0.01795	1	0.680	0.140	0.130
9	8.60	42.9	0.399	2574	0.02226	8	0.860	0.120	0.160
9	8.60	31.9	0.221	1914	0.02994	30	0.940	0.130	0.190
9	6.98	66.5	0.960	3990	0.01167	0	0.380	0.170	0.130
9	6.98	53.2	0.614	3192	0.01458	1	0.600	0.150	0.150
9	6.98	42.9	0.399	2574	0.01808	2	0.790	0.130	0.190
9	6.98	42.9	0.399	2574	0.01808	4	0.800	0.120	0.180
9	6.98	31.9	0.221	1914	0.02432	28	0.920	0.140	0.190
9	5.39	66.5	0.960	3990	0.00900	0	0.330	0.140	0.150
9	5.39	53.2	0.614	3192	0.01125	0	0.520	0.130	0.140
9	4.29	66.5	0.960	3990	0.00717	0	0.230	0.150	0.120
9	4.29	53.2	0.614	3192	0.00896	0	0.410	0.150	0.170
9	4.29	42.9	0.399	2574	0.01111	0	0.540	0.140	0.180
9	3.53	66.5	0.960	3990	0.00589	0	0.240	0.160	0.160
9	3.53	53.2	0.614	3192	0.00737	0	0.390	0.140	0.180
9	3.53	42.9	0.399	2574	0.00913	0	0.500	0.150	0.180
9	3.53	31.9	0.221	1914	0.01228	2	0.740	0.170	0.270
9	2.21	31.9	0.221	1914	0.00770	0	0.520	0.210	0.290

U_s/U_o is mostly dependent on Z_p, supports the theoretical expectation that for fully turbulent flow the entrainment rate $v_o \propto U_s^3/g_i'$. This regime appears to be independent of Reynolds number because roughly the same V' versus Z_p was observed for all three valley sizes. However, it became evident that this *Re*-independent regime is not well defined by Re_o greater than some critical value. This section describes several alternative Reynolds numbers and compares their effectiveness at ordering a relationship between V' and Z_p. One of them is used to develop an explicit relationship including molecular diffusion enhanced entrainment, eqn. (3).

The primary valley Reynolds number, $Re_o = U_o h/\nu$, is an index for full-scale simulation of valley-scale flow patterns in the ambient flow above the pool; however, Re_o does not adequately characterize the laminar/turbulent nature of entrainment in the shear layer between deep pool and ambient fluid. To characterize this layer, we first considered $U_s(U_s^2/g_i')/\nu \propto U_o^3/(g_i'\nu)$; this does not work well in our case because $(U_s/U_o)^3$ varies greatly with Z_p. (During review it was discovered that $K = U_s^3/g_i'\nu$ had been proposed by Turner [12], based on the early work of Keulegan [2]; Turner suggested a transition to instability of the interface (turbulent flow) at $K \geqslant 500$.) Then it was noted that v_o has the same dimensions as kinematic viscosity, ν, and that results support $v_o \propto U_s^3/g_i'$ in the large-*Re* regime, so the "shear Reynolds number" was defined as $Re_s \equiv v_o/\nu$. Upon trial, Re_s was found to order the data much better than Re_o.

A third type of Reynolds number also came to mind, based on the ratio of v_o or U_s^3/g_i' to the outflow that might be expected due to molecular diffusion of the dense gas into the ambient flow. The thickness of the diffused layer would be proportional to $(\kappa w/U_s)^{1/2}$, where κ is the molecular mass diffusivity and w is the pool width. With velocities in this layer proportional to U_s we have $v_o \propto (\kappa w U_s)^{1/2}$ for molecular diffusion alone (no turbulent entrainment). Replacing U_s with the more measurable U_o and κ with ν, which is of the same order of magnitude as κ for gases, we found that the combination $Re_f = v_o(U_o^3/g_i')/(\nu W U_o) = v_o U_o^2/(g_i' W \nu)$ worked well for our situation. We attribute this partly to the fact that U_o^2/W is proportional to U_s^2/w within $\pm 20\%$ over a wide range of pool depth, $Z_p = 0.3$ to 0.9, for our valley geometry, using $w/W = Z_p$ and the U_s/U_o relationship derived in the next section. Note that $Re_f \propto Fr_o \cdot Re_s$, and also that $Re_s = V_o \cdot Re_o$. Therefore, at fixed values of Fr_o, V_o, and h/W, all Reynolds numbers are proportional to the valley scale raised to the 3/2 power.

Figures 4 and 5 demonstrate the effectiveness of Z_p and Fr_o, Re_o, Re_s, or Re_f values for ordering measured V' values. Figure 4 shows the relative pool height, $Z_p = z_p/h$, versus $V'^{1/3} = (v_o g_i')^{1/3}/U_o$ with the symbols divided among ranges of Re_s. We find that for $Re_s > 30$ or so the points all cluster; i.e., Z_p is essentially a function of V' alone, or $v_o = U_o^3/g_o'$ times a function of Z_p. (We chose $V'^{1/3}$

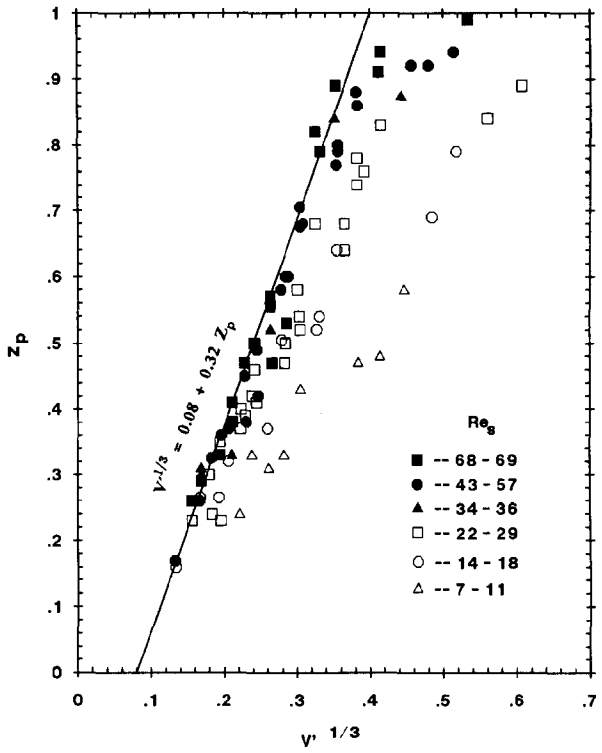

Fig. 4. Z_p vs. $V'^{1/3} = (v_o g'_i)^{1/3}/U_o$ with data stratified by Re_s.

for the abscissa because this made the high-Re plot almost linear.) A similar plot using Re_f ranges showed almost identical clustering for $Re_f > 1$.

We interpret this result to mean that $v_o \propto U_s^3/g'_i$, as predicted in Section 2 for fully turbulent flows with sufficient fetch for entrainment-limiting ($Fr_o < 1$, approximately), with U_s/U_o essentially a function of Z_p alone. In other words, in the large-Re, non-overflow situation, we think that $v_o \propto U_s^3/g'_i$ and that when $v_o = v_i$ the pool level adjusts itself to find the U_s that balances entrainment with the inflow rate, v_i. The high-Re_s data of Fig. 4 are fit fairly well by $V'^{1/3} \simeq 0.08 + 0.32\,Z_p$, except when $Z_p > 0.9$ (overflow cases). With $V' = v_o g'_i/U_o^3$ and the result of Section 6, $v_o \simeq 0.05\ U_s^3/g'_i$, we infer that $U_s/U_o \simeq 0.22(1+4\,Z_p)$ in the range $0.2 < Z_p < 0.9$ for this particular valley shape. It seems likely that "overflow" significantly increases v_o when $Z_p > 0.9$, but we have not attempted to quantify this regime.

Figure 5 demonstrates the relative effectiveness of Fr_o and the various Re at ordering V'. To eliminate significant overflow effects, the eight cases with $C/C_i > 0.1$ at the top of the valley are omitted. To reduce the significance of Z_p as an additional parameter, V' is divided by the large-Re approximation of Fig.

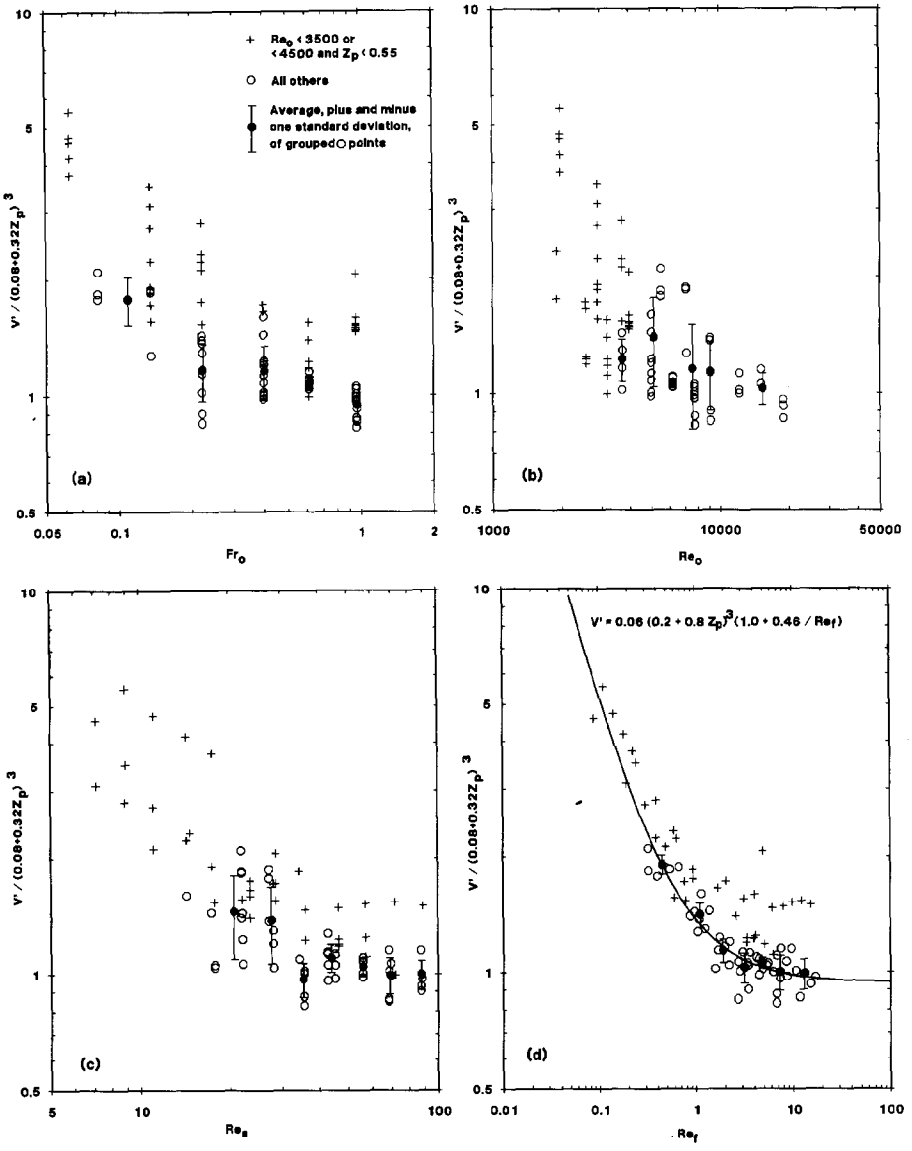

Fig. 5. $V'/(0.08+0.32\,Z_p)^3$ vs. (a) Fr_o, (b) Re_o, (c) Re_s, and (d) Re_f for cases with $C_{top}/C_i < 0.1$. Figure 5(d) shows fit of high Re_o data with eqn. (3), $V' = 0.06\ (0.2+0.8\,Z_p)^3\ (1+0.46/Re_f)$.

4, $(0.08+0.32\,Z_p)^3$. When this is plotted against Fr_o or Re_o, (Figs. 5a and 5b), there is a strong trend toward larger V' at small values of the abscissa, but with much scatter. The plots against Re_s and Re_f (Fig. 5c and 5d) show a similar trend but with reduced scatter, especially for Re_f.

While Figs. 5(c) and 5(d) are satisfactory, we were puzzled about why the

highest tunnel speed, small-valley points were all outliers, with considerably enhanced V' in spite of relatively large Re_s and Re_f values. The answer may be in the relatively small Re_o, about 4000, for the same points. Therefore we tried flagging all $Re_o < 4500$ points with a different symbol, and found almost all of them were systematically higher than $Re_o > 4500$ points in the same range (a slightly relaxed flagging criterion, $Re_o < 3500$, appears to be satisfactory for the higher pool levels, $Z_p > 0.55$). We believe this to indicate that valley-scale, large-Re flow is not adequately simulated at such small Re_o. The larger Re_o points show much reduced scatter, outstandingly so for the $V'/(0.08+0.32\,Z_p)^3$ vs. Re_f plot (Fig. 5d). While $Re_f < 0.3$ points are excluded by this Re_o criterion, we find in Fig. 5(d) a trend towards less difference between large and small Re_o points as Re_f approaches 0.3. Furthermore, the larger Re_o points can be fit well with the simple expression

$$V' = 0.06(0.2+0.8\,Z_p)^3(1+0.46/Re_f) \tag{3}$$

At small Re_f, this is consistent with our prediction for entrainment due to molecular diffusion alone; $(v_o g_i'/U_o^3) \propto 1/Re_f = g_i' W\nu/(v_o U_o^2)$ and the proportionalities $U_s \propto U_o$, $w \propto W$, and $\kappa \propto \nu$ yield $v_o \propto (\kappa w U_s)^{1/2}$. We will interpret this result further in the next section.

Although the main concern of this paper is the entrainment rate, the thickness of the mean concentration profile is of some interest. If this thickness,

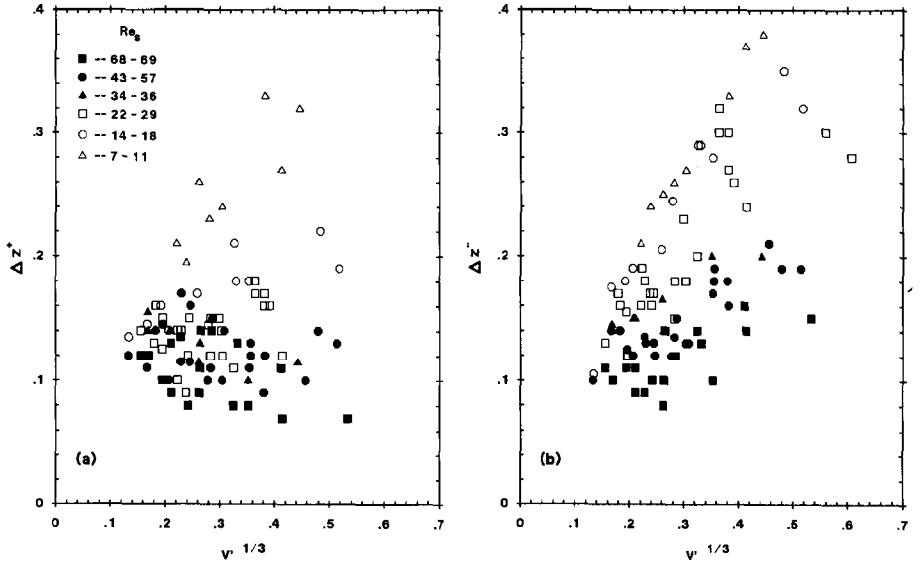

Fig. 6. (a) ΔZ^+ = thickness/h from $C/C_i = 0.1$ to 0.5 and (b) ΔZ^- = thickness/h from $C/C_i = 0.5$ to 0.9 vs. $V'^{1/3}$ with data stratified by Re_s.

Δz, were due to the entrainment zone, the estimate of Section 2 suggests that $\Delta z \simeq 0.3\ U_s^2/g_i'$ at large Re. Combining this with a result from Section 6, $v_o \simeq 0.06\ U_s^3/g_i'$, we calculate $\Delta z/h \simeq 2V'^{2/3}Fr_o$; for our data, this ranges from about 0.02 to 0.1, whereas the observed $\Delta z/h \simeq 0.2$ and was nearly constant with V' and Fr_o for the high Re experiments. Thus, the observed Δz could not be primarily due to the entrainment zone. The addition of smoke to the CO_2 during a few trials revealed waves of this magnitude, which probably account for most of the thickness of the time-averaged concentration profiles. We attempted to empirically correlate this observed thickness with the dimensionless variables, but did not have much success. For instance, we plotted upper and lower concentration profile thicknesses, divided by h (ΔZ^+ and ΔZ^-, respectively), versus V' with the symbols divided into various ranges of the variables used in Fig. 5. (At large Re, V' strongly correlates with Z_p (Fig. 4), so any relationship in V' implies a relationship in Z_p also.) Figure 6, the plot by Re_s category, was the best of these attempts. While there are some fairly well-defined trends with Re_s, there is much scatter in almost every range.

6. Determination of entrainment rate

Having established effective Re criteria for $v_o \propto U_s^3/g_i'$ and proved indirectly the validity of this relationship for large Re, assuming that U_s/U_o is a function of relative pool depth, we wished to quantify the above proportionality more directly. Towards this end, eight $Fr_o - V_o$ combinations were re-run in the medium valley with simultaneous mean speed profiles measured at the same mid-valley position used for concentration profiles; two of these are omitted from Table 4 because molecular diffusion effects may be too large, with $Re_f \leqslant 0.3$. All experiments were done using CO_2 ($g_i' = 512\ cm^2/s$). An example is shown in Fig. 7. It should be noted that, at depths where C/C_i exceeded a few percent, $u(z)$ became too small for reliable measurement with our instrumentation. Above this level, a safe and sure definition of U_s was nearly impossible to devise, given the constant increase of u with z.

We tried various ways to define the height of a characterizing "shear" speed, U_s, looking for definitions that produced the least scatter. Three of these U_s candidates are compared in Table 4. At $C/C_i = 0\%$, U is the mean wind speed at the lowest level above the dense gas where $C = 0$, or, at least, $C/C_i < 0.5\%$; this height is difficult to determine precisely. As $\partial C/\partial z$ rapidly steepens below this point, the $C/C_i = 1\%$ and 2% points were much easier to pinpoint, especially the latter. For comparability with the 0% height, fixed increments of height $= 0.02\ W$ and $0.04\ W$ were added to the 1% and 2% profile heights, respectively. These increments are about the same magnitude as turbulent vertical diffusion in the ambient flow over a fetch of $W/2$, so may describe an approximate height of effective flow coupling to the top of the density gradient.

TABLE 4

Normalized entrainment rates, various choices of U_s

Experiment	1	2	3	4	5	6	mean	std. dev.(%)
U_o, cm s^{-1}	66.4	53.5	53.5	53.5	39.8	39.8		
v_o, cm^2 s^{-1}	6.84	8.46	8.46	4.25	6.84	4.25		
Re_f	5.61	4.50	4.50	2.26	2.02	1.25		
Z_p	0.45	0.68	0.71	0.46	0.88	0.68		
U, cm s^{-1} at height where								
C/C_i=0%	47.5	45.5	43.5	36.0	34.5	32.0		
=1%+0.02W	47.0	43.0	40.0	33.0	34.5	32.0		
=2%+0.04W	44.0	43.5	43.0	33.0	36.0	34.0		
$v_o g_i'/[U_s^3(1+0.46/Re_f)]$, using $U_s=U$ at height where								
C/C_i=0%	0.030	0.042	0.048	0.039	0.070	0.049	0.046	26
=1%+0.02W	0.031	0.049	0.061	0.050	0.070	0.049	0.052	23
=2%+0.04W	0.038	0.048	0.049	0.050	0.061	0.041	0.048	16

As Table 4 shows, the U values measured at these three heights are comparable within $\pm 5\%$ or better, but the calculated values of $v_o/g_i'/U_s^3$, being sensitive to measured speed, show least scatter when based on $U_s=U$ measured at the 2% level plus $0.04W$. This calculation also includes the term $(1+0.46/Re_f)$, borrowed from eqn. 3, because the Re_f effect is still of some significance in this experimental range (Re_f=1.25 to 5.6).

On the basis of this table, reinforced with the Re_f term of eqn. (3), we suggest

$$v_o \simeq 0.05\ (U_s^3/g_i')(1+0.46/Re_f) \tag{4}$$

as a fit to our CO_2 experiments. The large-Re_f asymptote of this expression, $0.05U_s^3/g_i'$, is in agreement with the crude estimate of v_o made in Section 2 on the basis of Thorpe's [13] experiments. However, the definition of U_s remains an unsettled matter except in a very idealized flow situation, like that of Thorpe's experiment. A modest change in the selected height of wind speed measurement of $0.02h$, which is typical of differences in measured Z_p of our repeated experiments, changed U^3 by roughly 10% in most of the Table 4 runs. Thus, error in the coefficient "0.05" of eqn. (4) could easily be $\pm 20\%$.

We would like to generalize eqn. (4) by replacing U_o in the Re_f term with U_s and, also, replacing ν with κ, as the Re_f dependence is based on an expected molecular diffusivity effect rather than molecular viscosity. For CO_2 diffusing into air at 20°C, $\kappa \simeq 0.159$ cm^2/s, and is almost equal to ν, but κ and ν may be considerably different for other gases and are orders of magnitude different for liquids (as in the experiment discussed in the appendix). Because the molecular diffusion contribution to v_o is expected to be proportional to $(\kappa w U_s)^{1/2}$,

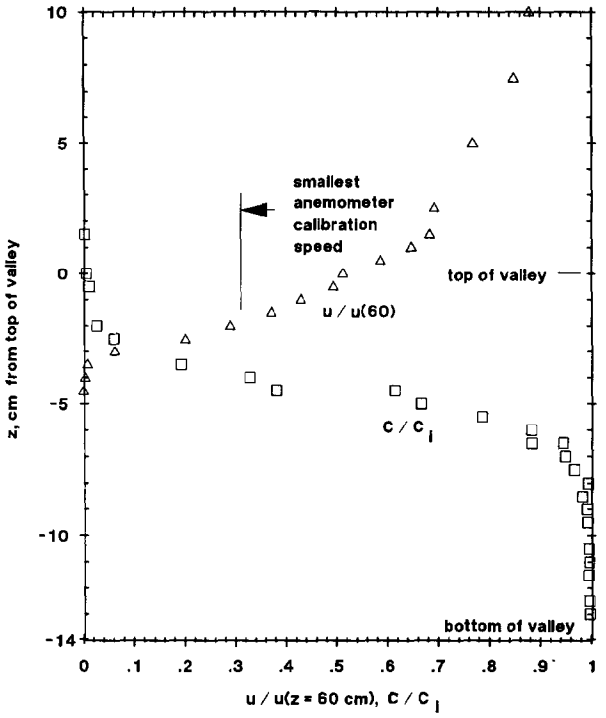

Fig. 7. Examples of mean profiles of u and of C/C_i at midpoint of valley during steady-state experiments.

where w is the dense gas pool width, we should also replace W in the Re_f term with w; for our triangular-shaped valleys, we replace W in the Re_f term with w; for our triangular-shaped valleys, we simply use $w/W=Z_p$. Comparing eqn. (4) with eqn. (3), we infer that $U_s/U_o \simeq 0.213(1+4Z_p)$. We can then use the approximation $(W/U_o^2)/(w/U_s^2) \simeq 0.045(1+4Z_p)^2/Z_p \simeq 0.88$ (within a factor of 1.21 over our experimental range, $0.2<Z_p<0.9$), and replace $Re_f^{-1} = g_i' \nu W/(v_o U_o^2)$ with $0.88\ (0.15/0.159) g_i' \kappa w/(v_o U_s^2)$. We substitute this into eqn. (4) and solve the resulting quadratic equation for v_o to get generalized, and potentially versatile, result

$$40\, v_o g_i'/U_s^3 \simeq 1+(1+30\, \kappa w\, g_i'^2/U_s^5)^{1/2}. \tag{5}$$

7. Flushing experiments

These experiments were intended to address the question of how long it takes to ventilate a low-lying area in the event of an accidental release of toxic, dense gas into the area. The most likely scenario is a sudden release rather than a continuous leak, and the removal process is anything but steady-state.

Consequently, a principal goal of our experiments was to monitor the rate of removal of dense gas as a function of time from a valley that is initially completely filled with dense gas, with no further inflow after flow initialization. The sliding cover valley model (cf. Section 3) allowed filling of the valley with no removal by entrainment until the cover was removed. The cover was slid open in a fraction of a second, with virtually no visible disturbance of the dense gas (as observed with smoke added). This provided a relatively well-defined initialization point, although it still required 3 to 5 s for the flame ionization detectors to register the full concentration after the gas traveled through the tubes connecting them to the sampling rake. The method used to obtain the concentration-weighted removal flux, v_o, was described in Section 3.

The steady-state experiments analyzed in the previous two sections can be used to provide a crude prediction for removal rate, so that the results of the two types of experiments can be compared. The data also provide effective Reynolds number criteria for determining at what point the removal by entrainment becomes influenced by viscosity and molecular diffusion (as the depth of the dense gas pool remaining in the valley becomes shallower, it usually reaches a level where U_s and v_o are too small for fully turbulent entrainment at the gas interface). We apply the steady-state experimental results by assuming that the removal rate v_o is the same as it would be during a steady-state experiment, when $v_o = v_i$.

We seek a model for z_p and v_o versus time. We can connect these two quantities by making a simplifying approximation that $C=0$ above z_p and $C=C_i$ below z_p. Then for the V-shaped valley, the total volume of remaining dense gas, at $C=C_i$, per unit length of valley is given simply by $A=A_oZ_p^2$, where A_o is the total cross-sectional area of the triangular valley section (Figs. 1 and 3). Then

$$v_o = -\mathrm{d}A/\mathrm{d}t = -A_o \mathrm{d}Z_p^2/\mathrm{d}t \tag{6}$$

We can easily solve this for the fully turbulent case by using eqn. (3) with $Re_f = \infty$:

$$V' = 0.06\ (0.2+0.8Z_p)^3$$
$$= v_o g_i'/U_o^3 = -(A_o g_i'/U_o^3)\mathrm{d}Z_p^2/\mathrm{d}t$$

We define a characteristic flushing time $t_f = A_o g_o'/U_o^3$ and $T = t/t_f$. The above is easily integrated, resulting in

$$Z_p = 1.25q - 0.25, \tag{7}$$

where $q = (5+(16-T/5.2)^{1/2})/(9+T/5.2)$

We have set the initial condition as $Z_p = 1$ at $T=0$. However, it is important to note that eqn. (3) is not valid for $Z_p > 0.9$ or < 0.2. When $Z_p > 0.9$, we observed 1.3 to 2.5 times as large v_o as given by eqn. (3) (see Fig. 4), an occurrence we

believe is due to "overflow", forcing of the pool over the downwind edge of the valley by shear stress acting on its surface. This is very transient and we did not attempt to model the removal rate for $Z_p > 0.9$, but we might expect that our prediction below for v_o will underpredict the initial peak in v_o, caused mostly by simple overflow.

Disregarding these caveats, we obtain a v_o prediction by substituting eqn. (7) into $V' = 0.06(0.2 + 0.8Z_p)^3$, obtaining

$$V' = 0.06q^3 \tag{8}$$

Repeating the above cautions, we can not expect this equation to be valid when $Z_p > 0.9$ ($T < 4$, approximately) or when $Z_p < 0.2$ ($T > 58$, at which point V' in eqn. (8) reduces to less than 5% of its initial value). We also do not expect it to be valid when the Reynolds number based on V' gets too small. Equation 3 gives $V' \propto (1 + 0.46/Re_f)$, so we can say that eqns. 7 and 8 are not valid if $Re_f < 1$, as a rough standard. We defined $Re_f = v_o U_o^2/(g_i' W\nu) = V' U_o^5/(g_i'^2 W\nu)$, and for the sliding door valley $W = 68$ cm. For CO_2 gas, this gives $Re_f = V'(U_o/19.3\ \mathrm{cm/s})^5$; thus, the value of V' defining $Re_f = 1$ depends very strongly on U_o.

Table 5 gives the principal variables for the five series of flushing experiments. The CO_2 experiments were done at four different wind speeds ranging over almost a factor of 2, so t_f varied by about a factor of 8 and V' at $Re_f = 1$ varied by almost a factor of 30. $Re_f = 1$ is calculated to occur before the time $Z_p = 0.2$ is reached only for the lowest U_o series for CO_2 and the SF_6 series. We note that $Fr_o > 1$ at the two highest speeds for the CO_2 tests. This is higher than the maximum in our steady-state tests (0.96). According to the theoretical discussion in Section 2, at $Fr_o > 1$ there may not be enough fetch for turbulent entrainment to reach its full value.

Figures 8 to 12 show measured values of V' versus T for the five series of experiments listed in Table 5. Each is compared with the curve given by eqn. (8), which is dashed when the corresponding $Z_p < 0.2$. Each series of experiments consisted of five runs in the full V-shaped valley and five runs in the flat-bottomed valley, with a flat floor at $z = 7$ cm $= 0.56\ h$. Every set of five

TABLE 5

Principal variables, flushing experiments

Variable	CO_2 series at four speeds				SF_6 series
Tachometer	82	102	128	160	160
U_o, cm s^{-1}	57	70.5	88.5	113	113
t_f, s	1.17	0.62	0.314	0.151	1.24
Fr_o	0.51	0.78	1.22	2.00	0.24
Re_o	4750	5900	7400	9400	9400
V', $Re_f = 1$	0.0044	0.0015	0.00049	0.00015	0.0098

identical runs has been averaged in these figures. To compare V' measured for the flat-bottomed valley directly with V' from the full valley, we defined t_f by using the full valley cross-sectional area, $A_o = 425$ cm^2, for both. However, referenced to the full-valley geometry, we expect the flat-bottomed valley to "run out of gas" at $Z_p = 0.56$, which, according to eqn. (5), occurs at $T \simeq 21$. The entrainment of dense gas in the flat-bottomed valley should remain fully turbulent until the pool is nearly gone for all five series of experiments. Because velocity measurements could not be made simultaneously with concentration measurements to infer v_o, there is considerable uncertainty in v_o and V'. For instance, the initial slug of large concentration during the overflow stage might have been accompanied by a slowdown in the $u(z)$ profile at the intake point for the $C(z)$ measurements. To partially compensate for these uncertainties, we adjusted the magnitude of v_o by a constant factor in each series to make $\int v_o dt = A_o$, which is also to say $\int V' dT = 1$. (Because we used the full-valley A_o in defining t_f, for the flat-bottomed valley we required $\int V' dT = 1 - (0.56)^2 = 0.69$.) There is also an uncertainty of several seconds in

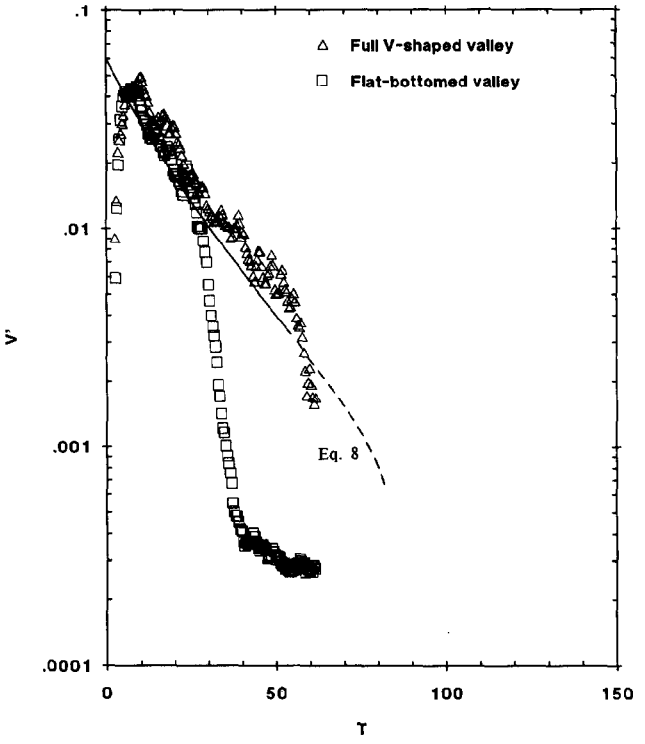

Fig. 8. $V' = v_o g_i'/U_o^3$ vs. $T = t/t_f$, where $t_f = A_o g_i'/U_o^3$ and A_o is the (full V-shape) valley cross-sectional area, for CO_2 at $U_o = 57$ cm/s ($Fr_o = 0.51$). Flat-bottomed valley floor is at 0.56 h above the bottom of the V-shaped valley. Eqn. (8) is plotted for comparison.

the starting time, because of the time it takes the gas to reach the sampling rake, 0.5 m downwind of the valley, and then to travel through about 5 m of tubing to the analyzers. This makes $T=0$ especially uncertain for the higher speed series. In terms of T, the time required for flow near the surface traveling at a speed $U_o/2$ to traverse the valley and reach the sampling rake is about 7 Fr_o.

In general the agreement between these data and the predictions derived as approximations of the steady-state experiments is good, especially for the three series with $Fr_o<1$. In Figs. 8, 9, and 12, for $Fr_o=0.51$, 0.78, and 0.24 (SF_6), respectively, the full-valley points approximate the eqn. (8) curve surprisingly well, even into the extrapolated ($Z_p<0.2$) part of the curve. Few of the data extend into the $Re_f<1$ regime (Table 5), and it appears to have little effect. The peak outflow was not measured until $T\simeq 8$, 5, and 6, respectively ($T=0$ is defined by the onset of measurable concentrations at the analyzers). This lag in response tends to mask any overflow effect on boosting V', if it occurred, and may offset the whole process in T somewhat. For instance, the flat-bottomed valley points show rapid decreases in V' beginning at $T\simeq 28$, 24, and 27,

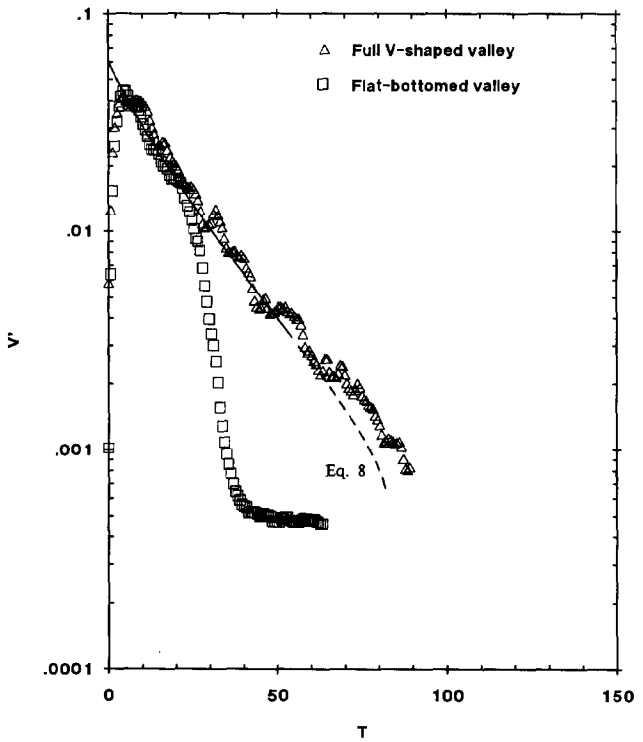

Fig. 9. V' vs. T for CO_2 at $U_o=70.5$ cm/s ($Fr_o=0.78$).

respectively, somewhat larger times than the predicted $T=21$ for the pool level to reach the level of the inserted floor, at $Z_p=0.56$. This depletion time displacement is quite comparable to the lag time. There was evidently some residual gas that took longer to diffuse out of the viscous sublayer adjacent to this floor and, possibly, some measurable residual that slowly leaked out of the inflow slot; this would explain why V' does not instantly plunge to zero as the pool level approaches the level of the inserted floor. Prior to this point of rapid decrease, the points from the flat-bottomed valley tests agree well with those from the full-valley tests, showing that the shape and size of the dense gas pool below its surface has little effect on the entrainment when $Fr_o<1$.

In Figs. 10 and 11, for $Fr_o=1.22$ and 2.00, respectively, the full valley points roughly approximate the eqn. (8) curve, as far as it goes, but show some rather substantial oscillations in V'. When $Fr_o>1$ the stress created in the shear layer is large enough to induce substantial motions in the dense gas pool, but the periods of oscillation seen in Figs. 10 and 11 are several times longer than would be expected of a seiche in a pool of this size. We note that the elapsed time between dips and peaks in V' vs. T is comparable to the time it takes to

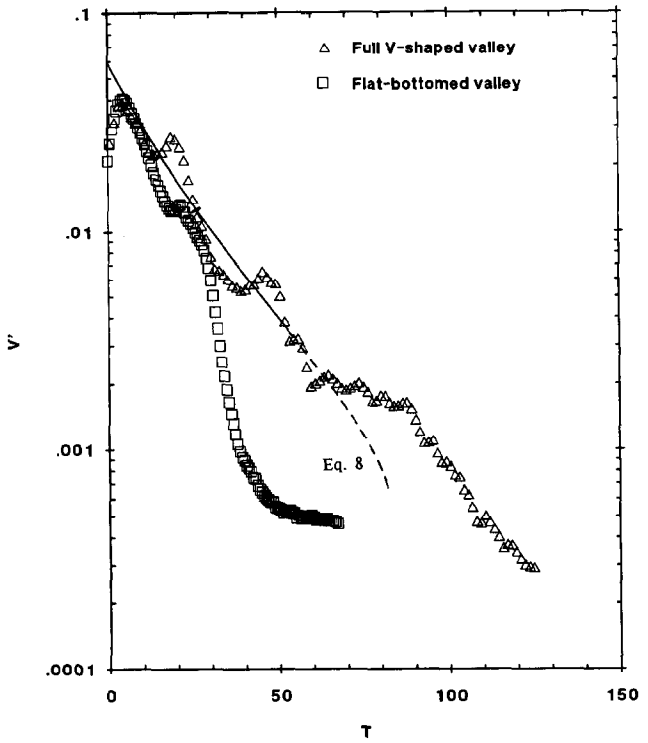

Fig. 10. V' vs. T for CO_2 at $U_o=88.5$ cm/s ($Fr_o=1.22$).

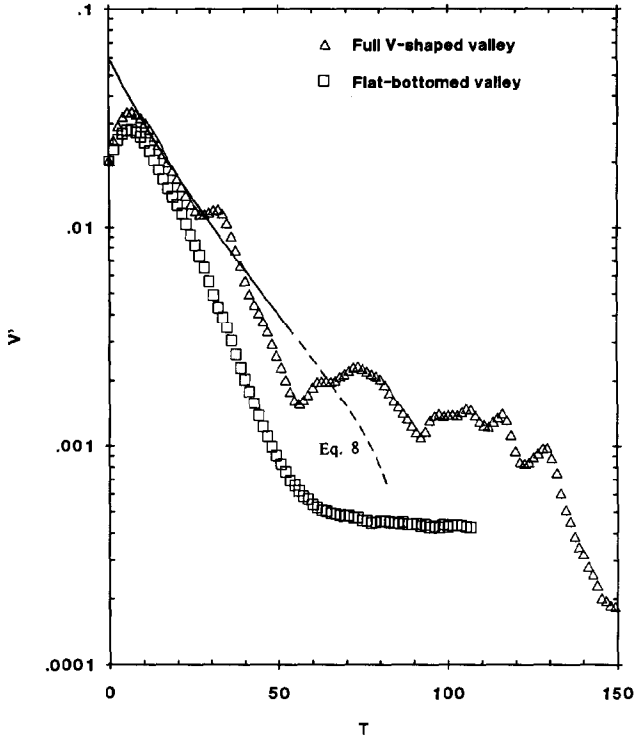

Fig. 11. V' vs. T for CO_2 at $U_o = 113$ cm/s ($Fr_o = 2.00$).

traverse the valley at a speed $U_o/2$, $\Delta T = 4\,Fr_o$. The flat-bottomed valley points describe dramatically smoother V' versus T functions, suggesting that the altered valley shape tends to dampen whatever oscillation was induced in the full V-shaped valley flows. There is only a slight suggestion of a secondary peak in V' in the $Fr_o = 1.22$ case (Fig. 10), followed by a rapid decrease beginning at $T \simeq 28$, similar to the $Fr_o < 1$ runs. The flat-bottomed valley points in the $Fr_o = 2$ case (Fig. 11) describe a very smooth curve, always below the curve of eqn. (8). This supports the speculation in Section 2 that the limiting value of entrained dense gas is not attained during the traverse of the pool if Fr_o much exceeds 1. Also, there is no point of sharp dropoff of V' vs. T in this case. The dropoff closely approximates an exponential decrease in T with a characteristic decay time $10.4\,t_f$, or $2.6\,W/U_o$, at this Fr_o. This is suggestive of diffusion of material out of a cavity in the wake of an obstacle, in which case nearly all of the material is circulated in the wake. That is, the dense gas "pool" may have been quickly destroyed by turbulent mixing at $Fr_o = 2$.

Figure 12, for SF_6 at $Fr_o = 0.24$, is especially interesting because SF_6 is a much denser gas than CO_2. Instead of $(\rho_i - \rho_a)/\rho_a = 0.52$, which can be consid-

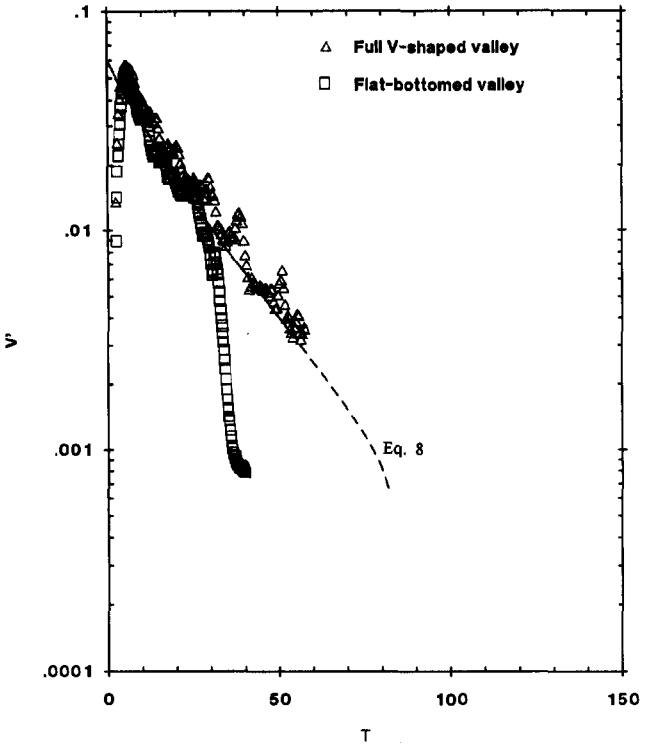

Fig. 12. V' vs. T for SF_6 at $U_o=113$ cm/s ($Fr_o=0.24$).

ered somewhat "small" compared to unity, $(\rho_i-\rho_a)/\rho_a=4.3$. Such large density differences might alter entrainment and other relationships that work well for small density differences. Nonetheless, the agreement of these data with eqn. (8) is surprisingly good.

8. Summary and conclusions

These experiments were carried out to determine the rate of removal of dense gases from topographic depressions by wind, with applications to accidental releases containing toxic gases especially in mind. Measurements were carried out in a large, boundary-layer wind tunnel using two idealized, two-dimensional shapes for the gas-trapping depression: full, V-shaped valleys set into the floor with their axes perpendicular to the wind, and the same shape with a flat floor inserted about mid-height, the flat-bottomed valley. Two different types of experiments were performed, steady-state and flushing experiments.

The steady-state experiments used preset values of steady inflow of CO_2 into the bottom of V-shaped valleys, with the tunnel speed adjusted in steps to

achieve preset values of the Froude number, Fr_o, based on approach flow speed and valley depth, h. Mean concentration versus height was measured at the valley midpoint under steady conditions, when it could be assumed that the outflow volume flux (per unit valley length) of CO_2, v_o, equaled the inflow flux, v_i. This enabled us to develop an entrainment rate relationship as a function of a reference height ($z=h/4$), approach flow wind speed, U_o, and of pooling depth, z_p, defined by the level of 50% concentration. For fully turbulent flows, we found that $v_o \simeq (U_o^3/g_i')(0.08+0.32\ Z_p)^3$, where g_i' is the relative density difference of the dense gas times gravitational acceleration and $Z_p=z_p/h<0.9$. When $Z_p>0.9$, we found 1.3 to 2.5 times larger v_o values, which we attribute to simple overflow of the dense gas pool, rather than entrainment.

Eight of these experiments were repeated, and detailed wind speed profile measurements made at the same mid-valley position to establish a more general entrainment relationship that was less dependent on valley shape. For sufficiently large Reynolds numbers (fully turbulent), we found $v_o \simeq 0.05\ U_s^3/g_i'$ when the shear speed U_s was defined as the mean wind speed at the lowest height over the pool where concentration equaled zero; because this level was difficult to determine precisely, we assign a $\pm 20\%$ uncertainty to this estimate. This is in good agreement with an estimate made in Section 2 on the basis of Thorpe's [13] experiments with water and brine in an enclosed, tiltable tube, a considerably different experimental configuration. Also in agreement with the theory in Section 2, this entrainment is limited by the weight of the dense gas and does not depend on valley or dense gas pool width, as long as $Fr_w<0.2$. (When $Fr_o \gg 1$, entrainment is rapid and the dense gas pool is removed relatively quickly.) Note that the above two entrainment relationships imply that, for this particular valley shape, $U_s/U_o \simeq 0.22(1+4Z_p)$, within the experimental limits $0.2<Z_p<0.9$.

The steady-state experiments were also useful for establishing Reynolds number criteria for fully turbulent flow, with *Re*-independent results. To broaden the *Re* range under otherwise identical flow conditions, these runs were made in three different-sized valleys, 50, 70, and 140 cm wide. We found that the *Re* based on approach flow and valley scale, $Re_o=U_oh/\nu$, did not order the observed entrainment rates very well, although v_o did tend to increase when $Re_o<4500$. A Reynolds number that was based on the entrainment rate itself, $Re_s=v_o/\nu$, ordered the data far better, with Reynolds number independent v_o at $Re_s>30$ to 60 (the larger threshold being at larger Z_p). The greatest success was with a more complex *Re* based on the ratio of turbulent $v_o \propto U_s^3/g_i'$ to v_o in a layer with speed proportional to U_s and thickness due to molecular diffusion alone, $\delta \propto (\nu w/U_s)^{1/2}$: $Re_f \equiv v_o U_o^2/(g_i' \nu W)$. Re_f was selected partly with the expectation that Z_p effects would be negligible, which turned out to be the case. We found the results practically *Re*-independent when $Re_f>2$. The results were ordered well enough to suggest an empirical fit of v_o including the molecular-diffusion regime (V-shaped valley), with

$$v_o \simeq 0.06 (U_o^3/g_i') (0.2+0.8 Z_p)^3 (1+0.46/Re_f) \quad (3)$$

The flushing experiments provided a separate test of the $Re_f = \infty$ (fully turbulent) part of the above relationship. These were performed in a valley with a sliding cover, which was opened smoothly and with little dense gas disturbance immediately after the valley was completely filled with gas and the gas shut off. In these experiments, the concentration profile was measured as a function of time at a point just downwind of the valley. Speed profiles were measured (not simultaneously) at the same point, and the integrated speed times concentration was used to infer v_o as a function of time. This $v_o(t)$ averaged over five runs was compared to a prediction made from the steady-state results, eqn. (3), for $Re_f = \infty$, by assuming that $v_o = A_o \mathrm{d}Z_p^2/\mathrm{d}t$, where A_o is the V-shaped valley cross-sectional area.

The resulting prediction (eqn. 8) generally compared well with the observed v_o versus t, especially for the three series with $Fr_o < 1$ (the regime addressed by the steady-state experiments). Unfortunately, there was a few seconds lag between the time measurable concentrations first reached the analyzers, taken as $t = 0$, and the time that peak concentrations were recorded. For the series run in a flat-bottomed valley, v_o dropped sharply at a time about equal to the above time lag plus the time predicted by eqn. (8) for the pool level to reach the valley bottom. A series run in both valley shapes with SF_6 at $Fr_o = 0.26$ gave very similar results, in spite of the much larger density than CO_2. For the two series run with CO_2 at $Fr_o > 1$, there were indications of a significant change in flow regime; there were substantial oscillations in v_o versus t for the full V-shaped valley experiments, and a smooth, exponential dropoff for the flat-bottomed valley series at $Fr_o = 2$.

The most generally useful result of this experiment is eqn. (3), modified to a form using the speed of the ambient flow just above the surface of the dense gas, U_s, instead of the reference speed U_o (U_o has meaning only for the V-shaped valley used in our experiments). The steady-state experiments made with wind speed profiles measured at the center of the dense gas pool support $V_o = 0.05 (U_s^3/g_i') (1+0.46/Re_f)$. We modified Re_f to a form of more general applicability, by using κ (molecular mass diffusivity), U_s and w (the pool width in the wind direction) in place of ν, U_o, and W. Using experimental proportionalities, we were able to rewrite the above result as

$$v_o \simeq 0.025 \ (U_s^3/g_i') [1 + (1 + 30 g_i'^2 w\kappa/U_s^5)^{1/2}] \quad (5)$$

Using eqn. (5), we suggest a criterion for molecular diffusion having less than 20% effect on v_o, in which case $v_o \simeq 0.05 \ U_s^3/g_i'$: $U_s > 2(g_i'^2 w\kappa)^{0.2}$, where κ is the coefficient of diffusion for the particular gas ($= 0.159 \ \mathrm{cm}^2/\mathrm{s}$ for CO_2 diffusing into air at 20°C). Note that this v_o has no dependence on dense gas pool width.

This assumes that w is sufficient for entrainment limiting by the weight of the entrained gas. In Section 2, we estimated a criterion for this condition as $w > 5\,U_s^2/g_i'$. For smaller w, the fully turbulent v_o may be reduced somewhat in proportion to w (our experiments did not cover this regime).

While we believe that eqn. (5) is a valid approximation for gases, with about $\pm 20\%$ uncertainty, it is not valid at low Reynolds numbers for similar flows in liquids when κ is orders of magnitude smaller than ν. As our analysis of Seeto's [11] experiment shows (see the appendix), at $Re_s < 30$ viscosity had a dampening effect on turbulent entrainment, while entrainment from molecular diffusion was negligible. At low Re, Seeto's data fit $v_o \simeq 0.002\,(U_s^3/g_i')^{1.45}\nu^{-0.45}$, while at $Re_s = v_o/\nu > 30$ or $K = U_s^3/(g_i'\nu) > 800$, they fit $v_o \simeq 0.04\,U_s^3/g_i'$. Part of the reason for the 20% smaller coefficient than for the large-Re part of eqn. (5) is that we were forced to use a different definition of U_s, due to the very different experimental configuration.

9. Applications of eqn. (5)

Two practical examples are given here for applications of eqn. (5). First, consider a "modest" spill of 1000 kg of chlorine gas (Cl_2, molecular weight = 70.9 g/mol, $\kappa = 0.143$ cm^2/s at 20°C) at ambient temperature into a holding pond 30 m square. This gives a 335 m^3 volume of gas at $g' = (70.9/28.9 - 1)\ 9.8$ m/s$^2 = 14.2$ m/s^2 and $w \simeq 30$ m for most wind directions. Then we can expect fully turbulent entrainment if $U_s > 2(14.2^2 \cdot 30 \cdot 0.0000143)^{0.2}$ m/s $= 1.23$ m/s. For a light wind of 1 m/s, we could use the full form of eqn. (5) to calculate $v_o \simeq 0.0051$ m^2/s; with $A_o = 335$ m^3/30 m $= 11.2$ m^2, the wind would evacuate the pond in a time $\simeq 40$ min. For diffusion beyond the pond, this practically could be treated as a continuous source of Cl_2. For the same example, a brisk wind would result in very rapid evacuation. For instance, at $U_s = 5$ m/s, $v_o \simeq 0.05(5^3/14.2)$ m^2/s $= 0.44$ m^2/s, which gives full evacuation in a time of about 25 s.

As a second example, consider a massive release like that of the CO_2 suddenly released from a deep lake in Cameroon, filling a 2-km wide valley about 10 m deep. (CO_2 is toxic at concentrations exceeding 10%, and killed several thousand people at distances up to 10 km down the valley from the lake [13].) We suppose $g' = 5.1$ m/s^2 and $A_o = 20{,}000$ m^2. At $U_s = 1$ m/s, molecular diffusion across a fetch of 2000 m is important; eqn. (5) gives $v_o \simeq 0.030$ m^2/s; thus, this wind would require about 8 days to evacuate the CO_2 from the valley! (Of course, we expect that other energy sources, such as surface heat flux, will do the job much faster.) At $U_s = 2$ m/s, turbulent entrainment dominates; $v_o \simeq 0.1$ m^2/s and evacuation would be accomplished by U_s in about $2\frac{1}{2}$ days. Even a strong valley crosswind of 10 m/s would take about half an hour to clear the valley of CO_2, too long for those caught by the release of a gas that can kill in minutes.

Finally, a more complex situation ought to be given brief consideration be-

cause it is potentially more common than topographically contained releases like those in our wind tunnel valley. Suppose a quick release of a volume Q_o of dense gas occurs in a valley of limited width, w, but with a nearly flat floor with plenty of room for gas to spread in the along-valley direction. In this case, we might borrow the result of Chen [14] for the two-dimensional spread of a buoyant gas released against a hard surface: $L \simeq 3.0(g_i' Q/w)^{1/3} t^{2/3}$, where L is the cloud dimension along the valley axis. The rate of depletion of the gas on the valley floor is then $dQ/dt = -v_o L$, where v_o could be estimated from eqn. (5). Integration of this equation gives $Q^{2/3} = Q_o^{2/3} - 1.2\ v_o\ (g_i'/w)^{1/3} t^{5/3}$, and the dense gas is completely removed by entrainment when $t \simeq 0.9\ v_o^{-3/5} Q_o^{2/5} (w/g_i')^{1/5}$. If $v_o \simeq 0.05\ U_s^3/g_i'$ (fully turbulent), then $t \simeq 5\ (Q_o g_i')^{2/5} w^{1/5} U_s^{-9/5}$. Again, U_s is the most critical factor; the total buoyancy of the release, $Q_o g_i'$, is the next most important factor, and the estimate of w is not critical at all.

If a similar release occurs in the daytime, or perhaps involves a cold gas released over a warmer surface, the total buoyancy could be depleted at a rate equal to the heat flux from surface to gas, H_o, times the surface area, wL. Defining $H^* = gH_o/(c_p \rho T_g)$, where c_p is the specific heat capacity of the gas and T_g is its absolute temperature, we can write $d(g_i' Q)/dt = -H^* wL = -3.0\ H^* w (g_i' Q/w)^{1/3} t^{2/3}$. Neglecting depletion of buoyancy due to removal by turbulent entrainment, this gives complete destruction of the initial negative buoyancy at a time $t \simeq 0.9\ (g_i' Q_o/w)^{2/5} H^{*-3/5}$. Comparing this to the turbulent entrainment removal rate derived at the end of the last paragraph, we find that the crosswind works faster than H_o only if $U_s > 2.7\ (H^* w)^{1/3}$. (Note: this speed very much resembles the "convective scale velocity", and does not depend on the release at all!) For instance, for solar heating, $H^* \sim 0.004\ m^2/s^3$ is typical; if $w = 1000$ m, then U_s must exceed 4 m/s for turbulent entrainment by valley crosswind to be the more effective agent for removing dense gas.

Acknowledgements

We thank Robert Lawson, Jr. (EPA)*, Michael Shipman (NSI Technology Services Corp.), and Paul Bookman (NSI) of the Fluid Modeling Facility and Ajay Kumar (North Carolina State University) for their roles in making this research effort possible. We also thank Barbara Hinton (EPA) for typing the manuscript.

*Although the research described in this article has been supported by the U.S. Environmental Protection Agency, it does not necessarily reflect the views of the Agency and no official endorsement should be inferred. Mention of trade names or commercial products does not constitute endorsement or recommendation for use.

Notation

A_o	cross-sectional area of valley, cm^2
C	local mean concentration of dense gas, $g\,cm^{-3}$
C_i	concentration of unmixed gas (initial or inflow value), $g\,cm^{-3}$
C_{top}	concentration of dense gas over valley at level of upstream surface, $g\,cm^{-3}$
Fr_e	$U_s^2/(g_i'\delta)$, Froude number for local entrainment layer
Fr_o	$U_o^2/(g_i'h)$, primary valley Froude number
Fr_w	$U_o^2/(g_i'W)$, Froude number based on valley width
g_i'	$g(\rho_i-\rho_a)/\rho_a$, modified gravitational acceleration, $cm\,s^{-2}$
h	valley depth, m
K	$U_s^3/(g_i'\nu)$, Keulegan number
q	$[5+(16-T/5.2)^{1/2}]/(9+T/5.2)$
Re_f	$v_o U_o^2/(g_i'W\nu)$, modified shear Reynolds number
Re_o	$U_o h/\nu$, primary valley Reynolds number
Re_s	v_o/ν, shear Reynolds number
t	time, s
t_f	$A_o g_i'/U_o^3$, characteristic flushing time, s
T	t/t_f
$u(z)$	mean wind speed as function of height, $m\,s^{-1}$
u_e	average entrainment velocity $(=v_o/w)$, s^{-1}
U_o	reference wind speed, measured at $z=h/4$ upwind of each valley, $m\,s^{-1}$
U_s	wind speed near surface of pool, $m\,s^{-1}$
v_i	volume inflow rate per unit length of dense gas into valley, $m^2\,s^{-1}$
v_o	volume outflow rate per unit length of dense gas leaving valley, $m^2\,s^{-1}$
V_o	$v_i/U_o h$, nondimensional inflow rate
V'	$v_o g_i'/U_o^3$ $(=v_i g_i'/U_o^3$ for steady state), primary nondimensional outflow rate
V_s'	$v_o g_i'/U_s^3$, shear nondimensional outflow rate
w	width of valley at top of dense gas pool $(=WZ_p$ for V-shaped valley), m
W	width of valley, m
x	coordinate in the downwind (cross valley) direction
y	coordinate in the lateral (along valley) direction
z	coordinate in the vertical, reference from bottom of valley or from upstream surface level
z_p	height of pool above bottom of V-shaped valley, m

Z_p	z_p/h
ΔZ^+	thickness (divided by h) of layer from $C/C_i=0.1$ to 0.5
ΔZ^-	thickness (divided by h) of layer from $C/C_i=0.5$ to 0.9

Greek

β	slope of side of valley, degrees
δ	entrainment layer thickness, cm
κ	molecular mass diffusivity, $cm^2\ s^{-1}$
ν	kinematic viscosity, $cm^2\ s^{-1}$
ρ_i	density of inflowing gas, $g\ cm^{-3}$
ρ_a	density of ambient fluid, $g\ cm^{-3}$

References

1 G.C. Christodoulou, Interfacial mixing in stratified flows, J. Hydraulic Res., 24 (1986) 77–92.
2 G.H. Keulegan, Interfacial instability and mixing in stratified flows, J. Res. Natl. Bur. Stand., 43 (1949) 487–500.
3 K. Lofquist, Flow and stress near an interface between stratified liquids, Phys. Fluids, 3 (1960) 158–174.
4 T.H. Ellison and J.S. Turner, Turbulent entrainment in stratified flows, J. Fluid Mech., 6 (1959) 423–448.
5 G. König, Windkanalmodellierung der Ausbreitung störfallartig freigesetzter Gase Schwerer als Luft, Institute of Meteorology, University of Hamburg, Hamburg, 1987, 105 pp.
6 C.M. Seeto, Ph.D. Thesis: An Experimental Study of Entrainment at a Density Interface by Mean Velocity Shear, Dept. Mech. Eng., University of Canterbury (New Zealand), 1987, 230 pp.
7 R.E. Britter and J.E. Simpson, Experiments on the dynamics of a gravity head current, J. Fluid Mech., 88 (1978) 223–240.
8 S.A. Thorpe, Experiments on instability and turbulence in a stratified shear flow, J. Fluid Mech., 61 (1973) 731–751.
9 R.C. Bell and R.O.R.Y. Thompson, Valley ventilation by crosswinds, J. Fluid Mech., 96 (1980) 757–767.
10 Snyder, W.H., The EPA Meteorological Wind Tunnel: Its Design, Construction, and Operating Characteristics, Report No. EPA-600/4-79-051, U.S. Environmental Protection Agency, Research Triangle Park, NC, 1979, 78 pp.
11 W.M. Pitts and B.J. McCaffrey, Response behavior of hot wires and films to flows of different gases, J. Fluid Mech., 169 (1986) 465–512.
12 J.S. Turner, Buoyancy Effects in Fluids, Cambridge University Press, Cambridge, 1973, 367 pp.
13 G.W. Kling, M.A. Clark, H.R. Compton, J.D. Devine, W.C. Evans, A.M. Humphrey, E.J. Königsberg, J.P. Lockwood, M.L. Tuttle and G.N. Wagner, The 1986 Lake Nyos gas disaster in Cameroon, West Africa, Science, 236 (1987) 169–175.
14 J.C. Chen, Studies on Gravitational Spreading Currents, Report No. KH-R-40, W.M. Keck Laboratory of Hydraulics and Water Resources, California Institute of Technology, Pasadena, CA, 1980, 436 pp.

Appendix

A similar experiment in a water channel

During analysis of our experimental data we learned of a similar experiment carried out at the University of Canterbury, New Zealand. We obtained a copy of the thesis detailing this experiment [6] during review of our paper. While the object of Seeto's experiment was similar to ours, there were some large dissimilarities also. First, the topographic depression was of a shallow, rectangular shape, which Seeto termed a "cavity". These cavities extended over almost the full width of the channel, hence were more truly two-dimensional, and had widths $W=3$, 9, and 29 cm in the flow direction. Because the wind stress on the dense fluid interface caused it to tilt significantly, it dropped as much as 1 cm below the upwind rim; this created a backflow region of significant dimensions, especially relative to the 3 and 9 cm cavities. Second, the ambient fluid was water and the dense fluids in the cavity were NaCl and CaCl salt solutions. While liquid mixing is dynamically similar to gas mixing at large Reynolds numbers, at small Re it is quite different because κ is about three orders of magnitude smaller than ν, whereas for gases like CO_2, $\kappa \sim \nu$. Third, Seeto's data analysis was philosophically different from ours, with no recognition of entrainment Reynolds number or of entrainment-limiting effects. To facilitate a comparison, we present below an abbreviated re-analysis of the data listed in Seeto's [6] appendices, but omit experimental details.

A major problem in comparing Seeto's experiment with ours is the choice of U_s, considering that our cavity shapes were quite different and that $\bar{u}(z)$ profiles were available only for upwind of Seeto's cavity. Obviously, our reference speed, U_o, would not be of comparable significance here. For the $W=29$ cm experiments the backflow region was relatively small, and Seeto's cavity could be considered essentially similar to a shallow pond of dense gas (or liquid). We opted for analysis in terms of U_s defined by $\bar{u}$ in the upwind profile at a height of effective mixing, δ, given by $d\delta/dt = ku^*$ and $dt = dx/U_s$, where $k=0.4$ is the Von Karman constant and u^* is the friction velocity, obtained here from a fit to the log profile law: $k\bar{u} = u^* \ln(z/z_o)$, where z_o is the effective roughness length. The result is the solution to $\delta(\ln(\delta/z_o)-1) = k^2 x$. We felt that this definition of U_s would be easier to transfer to the real world than the channel-defined bulk speeds used by Seeto (although we did obtain less data scatter when we tried using the whole-channel averaged speed). We applied this solution at $x = W/2$ to obtain $\delta = 0.6$ cm for $W=29$ cm. Another problem was that the speed at this height near the side walls of Seeto's channel was up to 1.3 times larger than at the center, due probably to the geometry of the suspended plate holding the cavity. We chose U_s measured at $\pm 1/4$ channel width from the center; this was roughly 1.07 times as large as the center speed.

For Seeto's $W=29$ cm experiments, $Fr_w \simeq 0.005$ to 0.1, considerably smaller than the 0.2 maximum we estimate for entrainment limiting in the fully tur-

bulent regime. Thus, we do not expect W to be a factor affecting v_o. At this small scale, we do expect Reynolds number effects. However, Re_o is not very relevant because of the shallowness of the dense fluid interface below upstream grade; neither is Re_f, because molecular diffusion was quite negligible in these fluids at experimental time scales ($\kappa \sim 10^{-3}\nu$, where for CO_2 and air in gaseous phase, $\kappa \sim \nu$). Re_s is relevant, as a measure of entrainment-layer eddy viscosity compared to ν. Therefore we plotted $v_o g_i'/U_s^3 = V_s'$ versus $Re_s = v_o/\nu$, obtaining Fig. 13 (we took v_o to be W times the mean entrainment velocity reported by Seeto). The result shows virtual Reynolds number independence when $Re_s > 30$ or so, with $v_o \simeq 0.04\ U_s^3/g_i'$; this is only 20% less than our result and our estimate from Thorpe's [8] experiment, both of which necessarily used very different definitions of U_s. At $Re_s < 30$ there is a strong Re_s effect, but the *opposite* sense of the effect observed in our experiment (see Fig. 5c). This we may attribute to the negligible molecular diffusivity in this case, and to the dampening effect of viscosity on turbulent entrainment at small Re_s.

To put this another way, we plot the same data as log V_s' versus log K in Fig. 14, where $K = U_s^3/(g_i'\nu) = Re_s/V_s'$. The small-$K$ regime is fit roughly by $V' = 0.002\,K^{0.45}$, or $v_o = 0.002\ (U_s^3/g_i')^{1.45}\nu^{-0.45}$. This is similar to Seeto's main

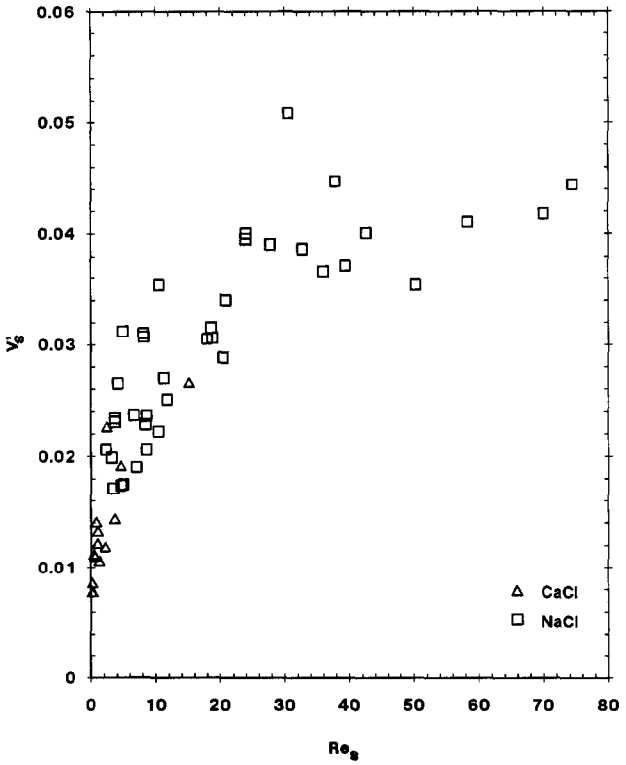

Fig. 13. $V_s' = v_o g_i'/U_s^3$ vs. Re_s for Seeto's [6] water channel experiment.

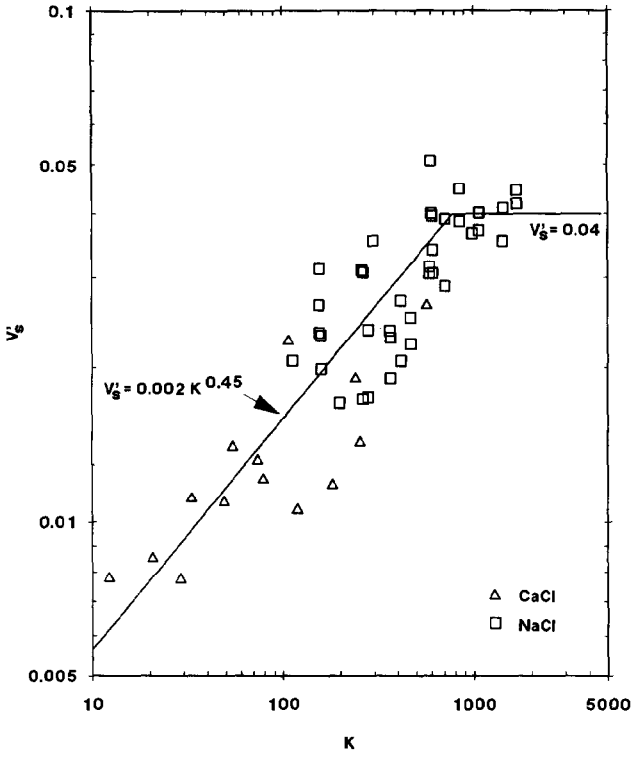

Fig. 14. V_s' vs. $K = U_s^3/(g_i' \nu)$ for Seeto's [6] water channel experiment.

result, although his analysis was in quite different terms (using entrainment velocity and Richardson number based boundary-layer thickness appropriate to a smooth, solid surface). In our terms, he obtained $v_o \propto U_o^{4.3} g_i'^{-1.5} \nu^{-0.3} W^{-0.2}$; of course W was constant, but g_i' varied by more than a factor of 20 and ν by a factor of 6. We note that the intersection of asymptotes in Fig. 14, at $K \simeq 800$, is not far from the critical value $K = 500$ suggested for the onset of instability by Turner [12].